Small calcium isotope fractionation at slow precipitation rates in methane seep authigenic carbonates

Clara L. Blättler*[a,b], Wei-Li Hong[c,d], Kalle Kirsimäe[e], John A. Higgins[b], and Aivo Lepland[c,d,e]

[a]Department of the Geophysical Sciences, University of Chicago, Chicago, IL, USA.

[b]Department of Geosciences, Princeton University, Princeton, NJ, USA.

[c]Geological Survey of Norway, Trondheim, Norway.

[d]Centre for Arctic Gas Hydrate, Environment and Climate, UiT The Arctic University of Norway, Tromsø, Norway.

[e]Department of Geology, University of Tartu, Tartu, Estonia.

*Corresponding author: cblattler@uchicago.edu

Abstract

Natural calcium carbonate minerals express a range of calcium isotope fractionations, with the precipitated mineral typically enriched in the lighter isotopes of calcium relative to source fluids. Experimental and theoretical evidence shows a strong dependence on precipitation rate, although this relationship has not been well quantified over the range of precipitation rates observed in natural settings. Endmember cases show that average marine carbonate precipitation expresses a large fractionation ($\delta^{44/40}$Ca values lower than seawater by approximately 1‰), while diagenetic carbonate phases assumed to have precipitated or recrystallized at very slow rates show negligible fractionation. The limited examples of quantified precipitation rates in natural settings with measurable, non-zero fractionation represents a barrier for applying mechanistic models of calcium isotope fractionation to geological applications. This study examines a methane seep system in the northern Barents Sea south of Svalbard where authigenic carbonate minerals are precipitating, driven by anaerobic oxidation of methane, and where the apparent calcium isotope fractionation factor and precipitation rate can be constrained by measuring properties of the pore fluids. Pore fluid profiles are analyzed in two shallow cores, and authigenic carbonate nodules are analyzed in one of these cores. The pore fluid profiles point to a transitional, non-steady state which approximates a closed system, where the elevation of pore fluid calcium isotope ratios through carbonate precipitation can be modeled as a Rayleigh distillation system. The apparent fractionation factors for ^{44}Ca/^{40}Ca ratios at these sites are α = 0.99985 and 0.9996, although the carbonate nodules suggest a different calcium isotope fractionation factor may have been expressed under past conditions. Precipitation rates at the two sites are estimated to be 1.4 and 3.5 μmol/m^2/h, intermediate between those of typical laboratory experiments and the much slower rates of marine diagenesis. Trace element analyses of the nodules (Mg/Ca and Sr/Ca ratios) suggest that both precipitation rate and mineralogy affect nodule composition. These results provide new constraints for the relationship between precipitation rate and calcium isotope fractionation and can inform modeling efforts leading towards mechanistic understanding of calcium isotope fractionation and trace element distributions in carbonate minerals.

1 Introduction

Natural calcium carbonate minerals show a wide spread of calcium isotope ratios, with $\delta^{44/40}Ca$ values of modern marine carbonates generally showing isotope fractionations between -1.8 to $-0.8‰$ from seawater (Skulan et al., 1997; Blättler et al., 2012; Fantle and Tipper, 2014). The source of this variability is not fully understood, but two dominant factors that have been shown to affect calcium isotope fractionation in controlled precipitation experiments are the $CaCO_3$ mineral polymorph (i.e. calcite or aragonite) and precipitation rate. The mineral polymorph effect has been observed in both natural and laboratory settings (Gussone et al., 2003, 2005; Blättler et al., 2012), with aragonite expressing greater calcium isotope fractionation than calcite. However, the effect of precipitation rate derived from laboratory experiments and theoretical models (Tang et al., 2008, 2012; Nielsen et al., 2012) has been challenging to demonstrate in the natural environment. End-member cases suggest that precipitation rate does indeed affect calcium isotope fractionation in the direction predicted by experiments and theory, with biogenic carbonates expressing fractionations on the order of $-1‰$ or greater (e.g. Skulan et al., 1997; Gussone et al., 2003, 2009), yet slow, diagenetic reactions apparently producing no isotopic fractionation (Fantle and DePaolo, 2007; Jacobson and Holmden, 2008). Recently, intermediate calcium isotope fractionations have been inferred from surface deposits at cold seeps in the South China Sea (Wang et al., 2012) and from a deep drillcore site off the west coast of South Africa (Bradbury and Turchyn, 2018), although uncertainties about fluid sources, advection, and diffusion in these settings prevent direct comparison to published calibrations with precipitation rate (e.g. Tang et al., 2008). The lack of documented calcium isotope fractionation at well constrained natural precipitation rates represents a limit to understanding calcium isotope variability in ancient carbonate rocks.

This study presents calcium isotope ratios for a methane seep system off the coast of Svalbard where the fractionation factor and precipitation rate for authigenic carbonate precipitation can be constrained by measurements of pore fluid properties, and then also compared to authigenic carbonate nodules grown over previous intervals of time. Previous calcium isotope measurements of carbonates from methane-associated sedimentary systems show large variability (Teichert et al.,

2005, 2009; Wang et al., 2012; Thiagarajan et al., 2020), but these datasets are not sufficiently well characterized (e.g. limited sampling resolution, lacking paired analyses of fluid and mineral phases) to effectively determine the relative importance of changing fractionation factors, pore fluid composition, and competing reactions within the sedimentary column. Here, sampling of pore fluids on a scale of 10s of centimeters as well as carbonate nodules recovered from one of the same cores allows for the sources of calcium isotope variability to be determined and for an exploration of authigenic carbonate precipitation on two different timescales. The specific history of pore fluid evolution at these sites, which are not presently at steady state but instead represent transitional, effectively closed systems (section 4.1), provides the opportunity to quantitatively estimate precipitation rates (section 4.3). Precipitation rates for authigenic carbonate are controlled by methane seepage and its anaerobic oxidation and are found to be at least an order of magnitude lower than those achieved in laboratory experiments (Tang et al., 2008). By capturing intermediate rates between the rapid precipitation characteristic of tropical biogenic carbonates and the slower rates of near-equilibrium diagenetic reactions, this natural experiment provides a link between the rate dependencies shown in experimental and theoretical studies of calcium isotope fractionation and those recorded in environmental settings. These results may then be used to test the predictions of mechanistic models of carbonate precipitation (e.g. Fantle and DePaolo, 2007; DePaolo, 2011; Nielsen et al., 2012), leading to better strategies for interpreting and extracting useful paleoenvironmental information from calcium carbonate archives.

2 Samples and methods

2.1 Core locations

The two sediment cores studied here were recovered from 386 m water depth at a seep field in the Storfjordrenna Trough ~50 km south of Svalbard (Fig. 1). The sediments of the Svalbard shelf generally consist of glaciomarine clay and silt (Andersen et al., 1996), and measured bottom water temperatures over the past several decades are between −2 and +5 °C (Hong et al., 2017). The

Table 1: Information about gravity cores collected in 2015 (Hong et al., 2017) and analyzed in this study.

cruise	core name	core recovery	water depth	latitude	longitude
CAGE15-2	940GC	3.10 m	386 m	76.1069°N	15.9779°E
CAGE15-6	1520GC	2.90 m	386 m	76.1057°N	15.9661°E

seafloor topography in the region shows mounds hundreds of meters wide with relief up to 10 m that bear evidence for current and past methane seepage (Hong et al., 2017). Evidence for active seepage at Storfjordrenna comes from hydroacoustic flares and bubble streams, and the evolution of methane seepage and pore fluid chemistry in the region has previously been studied by analysis of multiple gravity cores (Hong et al., 2017, 2018).

Gravity cores 940GC and 1520GC were recovered during two separate cruises in 2015 (see Table 1). Although active gas escape was not observed at either core site at the time of sampling, core 1520GC contained gas hydrates, and both cores bear authigenic carbonate nodules. Two nodules were reported from 940GC at 1.28 and 1.99 mbsf, and 26 nodules were reported from 1520GC between 0.46 and 3.48 mbsf (Hong et al., 2017). A sedimentary age model for the cores was derived from two radiocarbon ages of planktic foraminifera from an adjacent core, correlated to 940GC and 1520GC through results of X-ray fluorescence (XRF) scanning. Based on this age model, the sediments in the two cores date approximately from the onset of the last deglaciation through the Holocene with approximate sedimentation rates of 0.2 mm/yr. The youngest part of the Holocene appears to be missing at core 1520GC, possibly due to erosion (Hong et al., 2017).

2.2 Sampling

Pore fluids were recovered from both cores using acid-washed Rhizon samplers inserted into the cores. Fluids were collected into 20 mL acid-washed syringes and filtered through 0.2 μm cellulose acetate filters. Aliquots for cation analysis were acidified with 10 μL of reagent grade nitric acid, and those for carbon isotope analysis were poisoned with 10 μL of $HgCl_2$. Previous work has shown that sampling pore fluids with pre-wetted Rhizons yields accurate results for major ion concentrations, including calcium (Tada et al., 2015; Steiner et al., 2018), although small, systematic

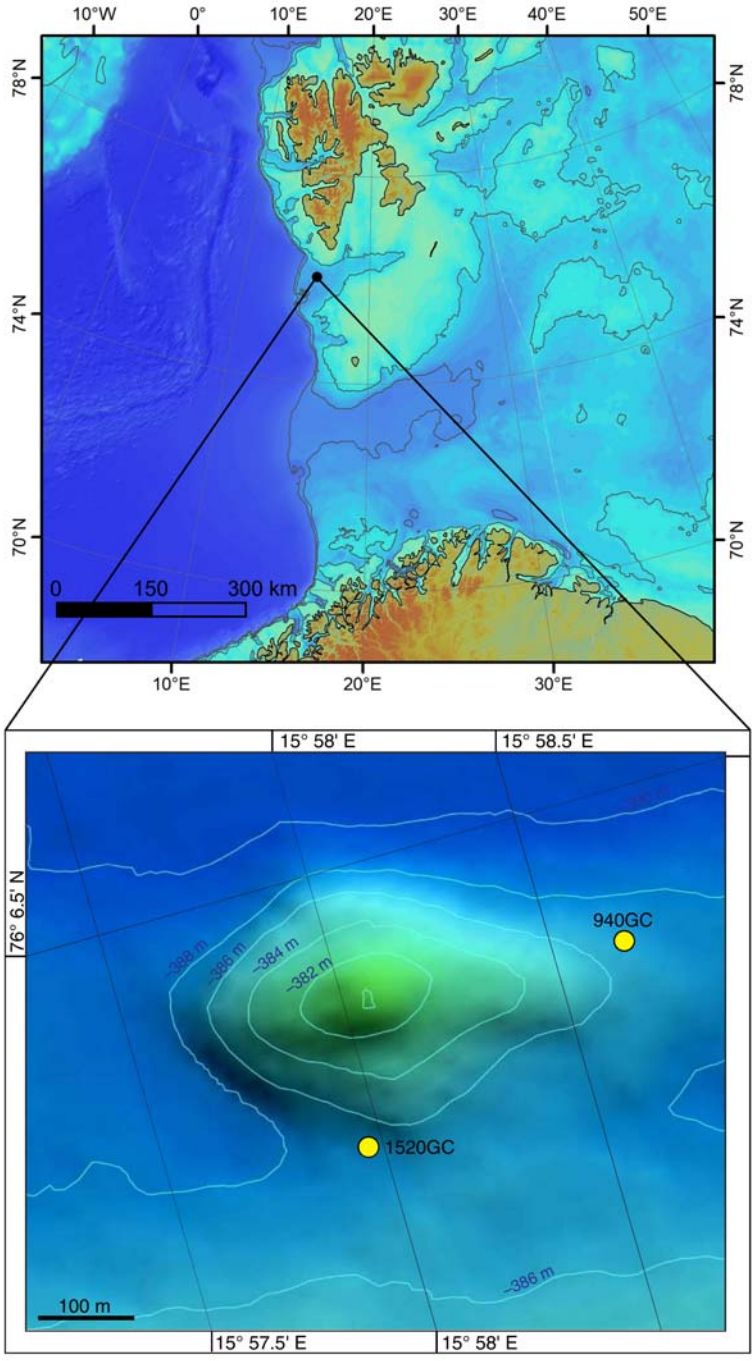

Figure 1: Regional map showing core sites on the edge of an actively discharging hydrate mound.

offsets have been observed for carbon isotope ratios (Steiner et al., 2018) and calcium isotope ratios (Wittke et al., 2020). Relative to centrifugation, pore fluids sampled with Rhizons were found to have elevated $\delta^{13}C$ values by approximately 0–1‰ (Steiner et al., 2018); relative to whole-round squeezing, Rhizon samples were found to have elevated $\delta^{44/40}Ca$ values by <0.1‰ (Wittke et al., 2020). These offsets, possibly driven by calcium carbonate precipitation and ion-exchange processes, do not affect assessments of relative changes within a pore-fluid profile, and can potentially be corrected by comparing the profile across the sediment-water interface to the composition of the bottom water (see section 3.1).

The geochemistry and mineralogy of six authigenic carbonate nodules from 1520GC were also analyzed. The six nodules, chosen from over 20 separate nodules identified in the core, were recovered between the depths of 0.52 and 3.38 mbsf. The weakly cemented nodules range in size from 0.3 to 4.0 cm, with irregular lumpy shapes (see Fig. 2). Direct radiometric dating of the carbonate minerals by U-Th isotope analysis (e.g. Crémière et al., 2016) is not possible because of abundant detrital components in the nodules contaminating the U-Th signal from the carbonate phases. Carbon isotope ratios ($\delta^{13}C$ values) of the six nodules were previously reported and range from −30.6 to −23.6‰ (Hong et al., 2017). Multiple subsamples were obtained from each nodule by drilling at different spots to obtain powders for calcium isotope analysis and quantitative mineralogical analysis by X-ray diffraction (XRD). The carbonate within nodules is mainly represented by authigenic precipitates, although a minor non-authigenic component of detrital dolomite and biogenic calcite debris (foraminifera) may also be present.

2.3 Geochemical analyses

The analysis of calcium isotope ratios for the pore fluids and carbonate nodules follows previously documented methods (Blättler and Higgins, 2017; Blättler et al., 2019). Carbonate powders were dissolved in 0.1 M acetic acid buffered with ammonium hydroxide to a pH of approximately 4.5 to minimize solubility of non-carbonate phases, then centrifuged and separated from the insoluble residue. Both pore fluids and dissolved carbonates were then prepared for isotopic analysis by sep-

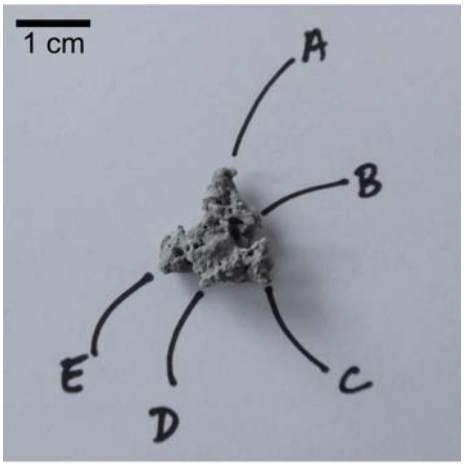

Figure 2: Carbonate nodule from 1520GC at 0.515 mbsf, showing a representative irregular shape and the locations of five subsamples (A–E) drilled for geochemical analyses.

arating calcium through automated ion chromatography. Samples were diluted with 0.2% HNO_3 to between 20 and 60 ppm Ca, and injections of 200 µL of sample were eluted through a cation-exchange column with methanesulfonic acid. Purified calcium solutions were then dried down, treated with concentrated HNO_3, dried down again, and diluted with 2% HNO_3 in preparation for analysis by multi-collector inductively coupled plasma mass spectrometry (ICP-MS). Mass spectrometric methods follow those reported in Blättler and Higgins (2017). Reported $\delta^{44/40}$Ca values are calculated from initial $\delta^{44/42}$Ca values using analyses of ^{44}Ca, ^{43}Ca, and ^{42}Ca and sample-standard bracketing with an in-house single-element ICP-MS calcium solution as the reference standard. These $\delta^{44/42}$Ca values are normalized to samples of modern seawater (SW) treated as samples and run in the same batch and then converted to $\delta^{44/40}$Ca values assuming exponential mass fractionation (Young et al., 2002) and no radiogenic ^{40}Ca excess. The long-term reproducibility of these laboratory methods for repeated analyses of carbonate minerals as well as seawater-matrix samples is identical at ±0.14‰ (2σ standard deviation), and the measured $\delta^{44/40}$Ca value of SRM915b relative to seawater is −1.15‰ (n = 199, 2σ = 0.14‰; identical within errors to reported values of −1.16 ± 0.08‰ (Heuser and Eisenhauer, 2008) and −1.13 ± 0.04‰ (Jacobson et al., 2015)). Data are reported relative to seawater (‰, or ‰ SW) and additionally presented relative to NIST SRM 915a (‰ 915a) using the published conversion: $\delta^{44/40}Ca_{915a} = \delta^{44/40}Ca_{SW} + 1.88‰$ (Hippler et al., 2003; Heuser et al., 2016).

Mineralogical and trace element analyses were also conducted on the subsamples of the carbonate nodules from 1520GC. The acetic-acid-soluble components of the samples were analyzed by ICP-MS using scandium as an internal standard. Elemental ratios relative to calcium are reported using external standards matrix-matched to a similar concentration of calcium (10 ppm). Repeat analyses of the carbonate standard NIST SRM 88b indicate analytical precision better than ± 5%. The mineralogical composition of powders from the same locations on the nodules was studied by X-ray diffractometry (XRD). The minute samples were pulverized by hand with an agate mortar and pestle under ethanol and preparations were made by dropping the sample suspension onto low-background silicon wafers. The mineralogical composition was interpreted and modeled using the Rietveld algorithm-based code Topaz by Bruker. The relative error of quantification, based on analyzing known, homogenized mixtures of rock-forming minerals, is better than 10% for major phases (>5 wt%) and better than 20% for minor phases (<5 wt%). Unit-cell parameters of calcite and Mg-calcite phases were obtained by using Rietveld structure refinement. The magnesium content ($MgCO_3$ mol%) of calcite was estimated from the unit cell *a* parameter according to Bischoff et al. (1983) and Zhang et al. (2010).

Carbon isotope measurements for dissolved inorganic carbon in the pore fluids were made in the Stable Isotope Laboratory at Oregon State University using a Finnigan GasBench-II headspace sampler with an online Finnigan DELTAplusXL gas-source isotope-ratio mass spectrometer (Torres et al., 2005). Pore fluids were sampled with a syringe and loaded into clean septum-capped vials that were then flushed with helium. The samples were acidified with phosphoric acid and the headspace gases were sampled, dried, eluted through a gas chromatography system, and fed directly into the isotope-ratio mass spectrometer. Carbon isotope ratios were normalized to multiple standards run before and after each sample and calibrated to known international standards. The average standard deviation for pore fluid $\delta^{13}C$ values measured with these methods is ± 0.04‰ (Torres et al., 2005).

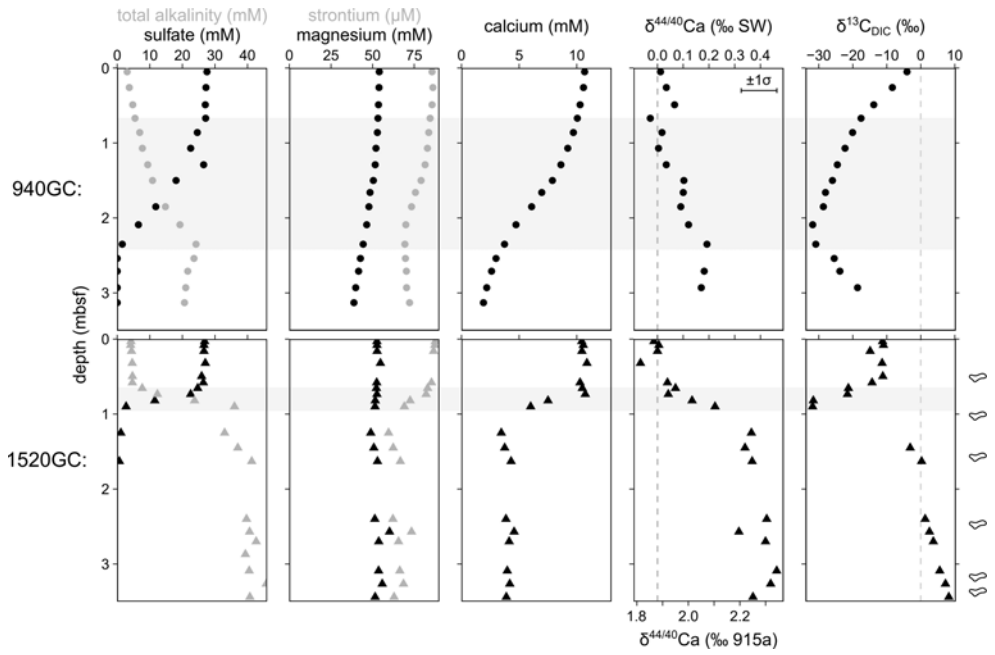

Figure 3: Pore fluid profiles from 940GC and 1520GC. Gray bands show the intervals of decreasing sulfate concentrations, including the modern sulfate–methane transition zone (SMTZ). Symbols at right show depths of nodules analyzed in this study. Calcium isotope ratios ($\delta^{44/40}$Ca values) and carbon isotope ratios (δ^{13}C values) are from this study; concentration data were previously reported in Hong et al. (2017) and Hong et al. (2018).

3 Results

3.1 Pore fluids

Pore fluid profiles for cores 940GC and 1520GC show many similar features, but differ in the depths at which geochemical changes occur as well as the extent and abruptness of these changes (Fig. 3, Table 2). In core 940GC, sulfate concentrations drop to zero between 0.8 and 2.5 mbsf (meters below sea floor) while total alkalinity rises to 24 mM. Magnesium and strontium concentrations decrease to 40 mM (26% decrease) and 70 μM (18% decrease), respectively. Calcium concentrations decrease smoothly from 10 to 2 mM over the 3 m length of the core. Calcium isotope ratios are close to zero in the upper part of the core, but increase slightly to 0.2‰ between approximately 1.5 and 2.5 mbsf. Carbon isotope ratios in DIC decrease steadily from −4‰ in the shallowest sample (0.05 mbsf) to a minimum of −32‰ at 2.1 mbsf, before rising at greater depths to reach −19‰ at 2.9 mbsf.

Pore fluids from core 1520GC show much more abrupt changes compared to 940GC, with transitions occurring at shallower depths and with steeper gradients. The drop in sulfate and increase in total alkalinity occur sharply between 0.7 and 0.9 mbsf. In contrast to 940GC, magnesium remains essentially constant with depth, but strontium concentrations also decrease to 63 μM (28% decrease). Calcium concentrations drop to 3 mM over the same interval that sulfate decreases, while calcium isotope ratios increase to 0.4‰. Carbon isotope ratios of DIC decrease with depth to −32‰, the same minimum value observed at 940GC, but at the much shallower depth of 0.9 mbsf. At greater depths in 1520GC, $\delta^{13}C$ values of DIC rise towards positive values, reaching 8‰ at 3.4 mbsf.

Based on comparisons between the shallowest pore fluid samples (5 and 3 cm below the sediment-water interface for 940GC and 1520GC, respectively) and the composition of seawater, there is no resolvable offset in major ion concentrations (Hong et al., 2017, 2018) or in calcium isotope ratios for pore fluids, indicating that pore fluid collection by Rhizons did not induce any sampling-related artifacts. The strong apparent gradient in carbon isotope ratios across the sediment-water interface prevents such a comparison and assessment of sampling artifacts for measured $\delta^{13}C$ values in the pore fluids, so a 0–1‰ offset towards more positive values (Steiner et al., 2018) may be present in the pore fluid $\delta^{13}C$ data presented here. However, the magnitude of this potential offset is small relative to the observed range in $\delta^{13}C$ values in the pore fluid profiles and would have a negligible effect on interpretations of these data.

3.2 Carbonate nodules

Mineralogical and geochemical data from the authigenic carbonate nodules from 1520GC show a composition dominated by Mg-calcite with Mg/Ca ratios ranging from 0.13 to 0.24 mol/mol (Table 3). The geochemical compositions are relatively constant among subsamples of an individual nodule. There is more variation across the set of nodules than within subsamples from the same nodule. Calcium isotope ratios range from −0.86 to −0.30‰ and are positively correlated with Mg/Ca ratios (r^2 = 0.77) with a weak inverse correlation with Sr/Ca ratios (r^2 = 0.44) (Fig. 4).

Compared to methane-derived carbonates recovered at seep sites in the Barents and North Seas (Thiagarajan et al., 2020), the samples from 1520GC show less geochemical variability in all measured properties (Fig. 4).

Quantitative mineralogical assessments from XRD match the predictions from the geochemical patterns (Table 3). Mg-calcite is the dominant carbonate phase, with only one subsample containing a substantial amount (> 1% of total carbonate) of aragonite. This subsample, which consists of 12% aragonite and 55% Mg-calcite, also has the most negative $\delta^{44/40}$Ca values measured in the nodules from 1520GC, −0.86‰, as well as the highest Sr/Ca and lowest Mg/Ca ratios. Minor dolomite (up to 3.7%) that could be either detrital or authigenic is also present in the nodules. Assuming that the calcium carbonate phases are mainly authigenic, 25–42% of each sample consists of detrital sediments, predominantly quartz, mica (clays), and plagioclase, with minor K-feldspar, chlorite, hornblende, and pyrite (in general order of abundance). These acetic-acid-insoluble phases were not dissolved by the treatments described above and do not contribute to the trace element and isotopic results. The composition of the detrital components is roughly constant across all the subsamples.

Previously reported δ^{13}C values of the nodules from 1520GC range from −31 to −23‰ (Hong et al., 2017). These are similar to δ^{13}C values of authigenic carbonates at other active and fossil methane seeps in the Barents and Norwegian Seas (Crémière et al., 2016; Thiagarajan et al., 2020).

4 Discussion

4.1 Evolution of subsurface conditions

The pore fluid profiles from these methane seep sites present special conditions that allow for calculating the effective calcium isotope fractionation and estimating precipitation rate at a specific moment in time. The concave-up and kink-shaped profiles in sulfate concentrations (Fig. 3) show that the flux of subsurface methane has increased recently (on the order of thousands and hundreds of years ago for 940GC and 1520GC, respectively) and that pore fluid profiles are still evolving to-

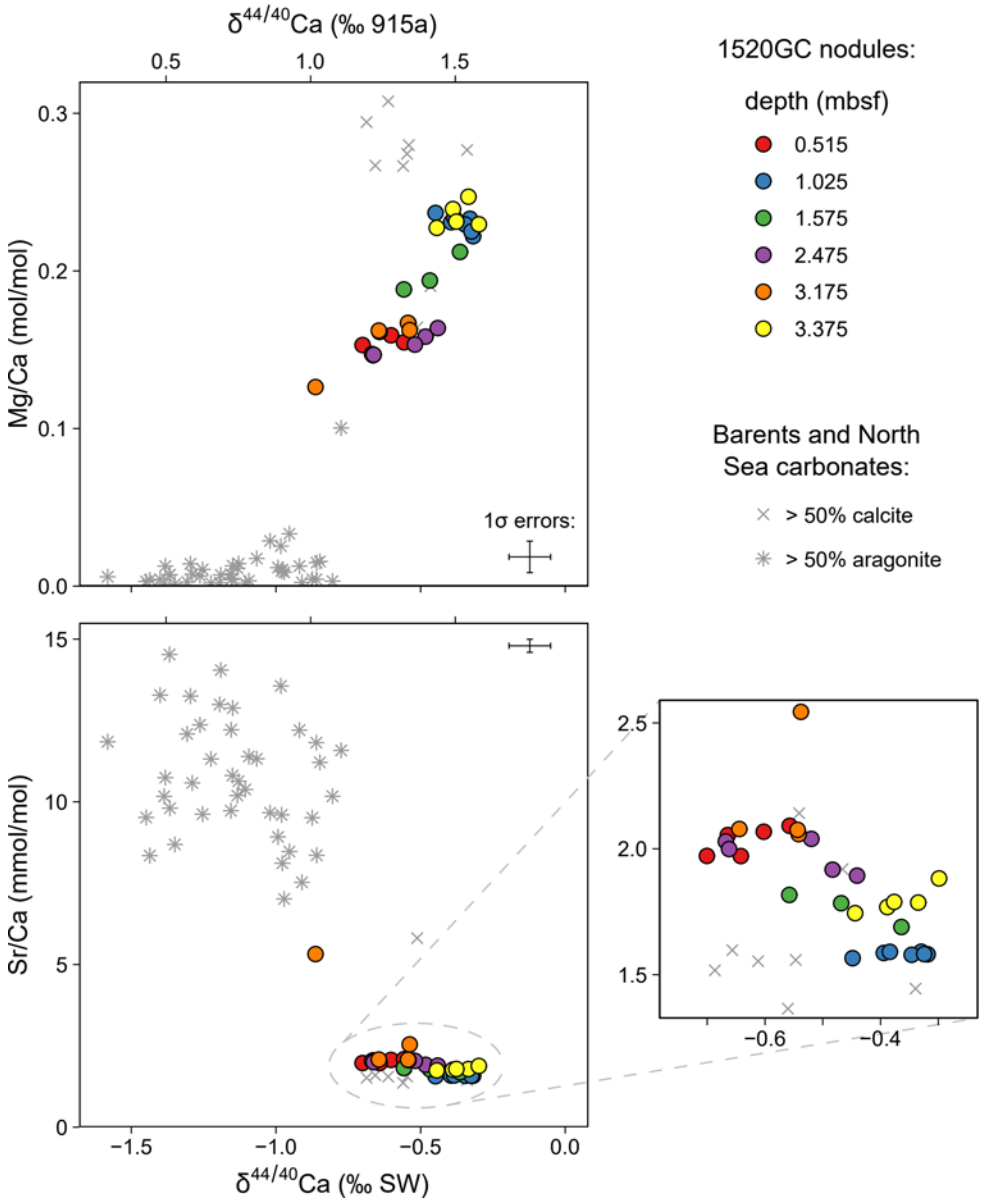

Figure 4: Geochemical properties of authigenic carbonate nodules from 1520GC (colored circles), compared to carbonate crusts from other methane seep sites in the Barents and North Seas (gray symbols) reported in Thiagarajan et al. (2020).

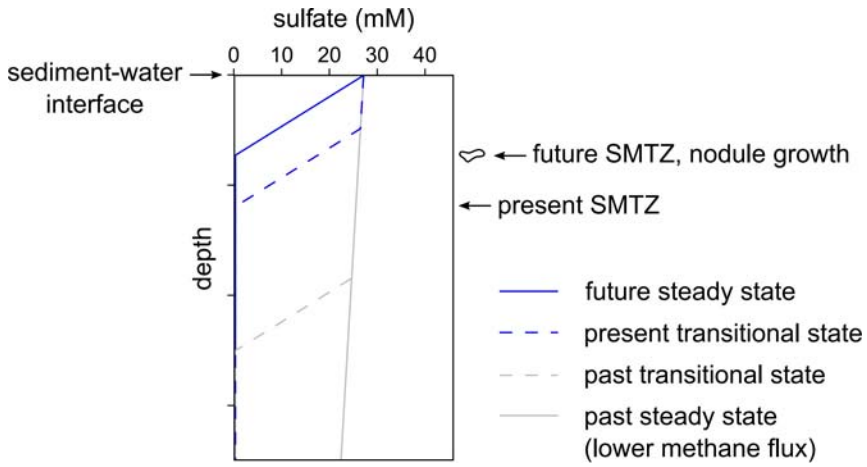

Figure 5: Idealized cartoon representation of pore-fluid evolution of sulfate concentrations and SMTZ migration at study sites. Authigenic carbonate nodules may form when the SMTZ occupies a depth interval for an extended period of time during steady-state conditions, with ions supplied by diffusion from above. During transitional states (including the state captured by the modern pore fluid profiles), carbonate mineral precipitation is volumetrically insignificant and effectively occurs in a closed system, where only ions that are already present in the pore fluids are consumed as the profile evolves upward towards a new steady state defined by a higher methane flux.

wards new steady states (Hong et al., 2017). At steady-state conditions, sulfate concentrations will be controlled by diffusion and decrease linearly with depth towards the sulfate-methane transition zone (SMTZ). In contrast, the non-linear profiles at these two sites indicate upward (and ongoing) migration of the SMTZ (Fig. 5). The rate of sulfate reduction and the location of the SMTZ at steady-state will be determined by the flux of methane from below. The excellent correlation between sulfate and calcium concentrations shows that sulfate reduction coupled to anaerobic oxidation of methane (AOM) leads to calcium drawdown through alkalinity production and precipitation of authigenic carbonate within the SMTZ.

Whereas pore fluid profiles capture a snapshot of presently evolving subsurface conditions, the authigenic carbonate nodules are the reaction products of conditions at these sites over longer intervals of time. The calcium concentration profiles indicate that carbonate minerals precipitate largely within and immediately surrounding the SMTZ, and therefore the depth range over which carbonate nodules are found reflects the past migration of the SMTZ through the sediment column. The SMTZ may move vertically either by accumulation (or erosion) of sediment or changes in the methane flux from below. For example, carbonate nodules found at shallower depths than

the present SMTZ at 1520GC could reflect erosion of sediment or a greater methane flux in the past (Hong et al., 2017). Mass balance considerations also require that the nodules grew over an extended period of time because the drawdown of calcium within the pore fluid profile can only account for a fraction of the carbonate present (in a closed system, the observed decrease of 7 mM calcium would yield less than a milligram of carbonate per cm^3). To grow nodules, calcium must ultimately be supplied by diffusion from the overlying seawater while the SMTZ occupies a particular interval at a stable methane flux level. For present-day fluxes (see section 4.3), growth of cm-scale nodules would require precipitation at the SMTZ over at least 10^2-year timescales.

The carbon isotope ratios of the carbonate nodules compared to DIC also demonstrate how the SMTZ must have migrated in the past. Minimum $\delta^{13}C$ values of $-32‰$ occur for DIC at the SMTZs of both 940GC and 1520GC, reflecting the active oxidation of ^{13}C-depleted methane at those depths. Carbonate nodules from 1520GC have $\delta^{13}C$ values ranging from -31 to $-23‰$; given a $1‰$ carbon isotope fractionation between DIC and calcite (Romanek et al., 1992), these nodules suggest pore fluid $\delta^{13}C$ values were between -32 and $-24‰$ during nodule growth. Measured $\delta^{13}C$ values in the DIC are much higher both shallower and deeper than the modern SMTZ (Fig. 6), indicating that the nodules did not grow under their present conditions, but rather in the past when the SMTZ occupied those sedimentary intervals (Hong et al., 2017). The range of nodule $\delta^{13}C$ values may reflect some limited assimilation of carbon outside of the SMTZ or a different balance of carbon sources (i.e. different proportions of methane-, organic matter-, and seawater-derived DIC within the SMTZ) in the past. The low $\delta^{13}C$ values of the nodules also confirm that detrital sedimentary carbonate (e.g. foraminifera or dolomite grains, with expected $\delta^{13}C$ values close to $\sim 0‰$) is negligible.

4.2 Interpreting pore fluid calcium isotope ratios

The drawdown of calcium as authigenic carbonate precipitates in 940GC and 1520GC fractionates calcium isotope ratios and shapes the pore fluid profiles of $\delta^{44/40}Ca$ values. In a closed system, the preferential removal of lighter calcium isotopes during rapid carbonate precipitation will en-

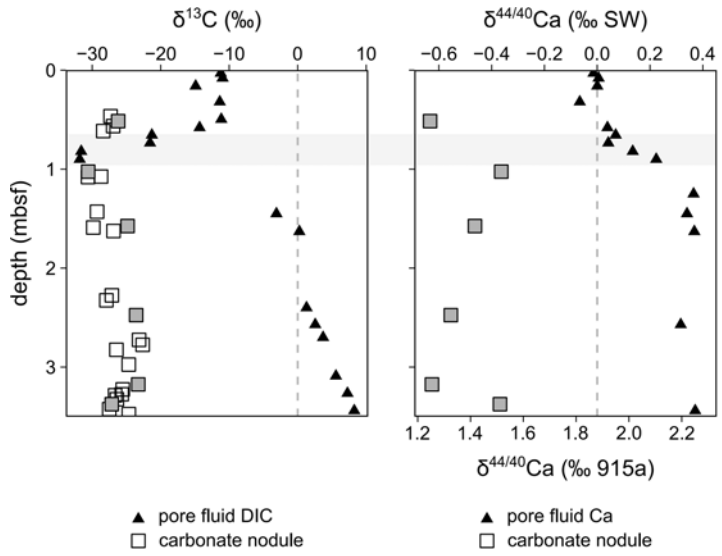

Figure 6: Comparison of carbon isotope ratios ($\delta^{13}C$ values) and calcium isotope ratios ($\delta^{44/40}Ca$ values) for pore fluids and authigenic carbonate nodules (average of multiple subsamples) at 1520GC. Filled squares indicate nodules with $\delta^{44/40}Ca$ values analyzed in this study (nodule $\delta^{13}C$ data previously reported in Hong et al., 2017).

rich pore fluids in the heavier isotopes through Rayleigh distillation, leading pore fluids to evolve towards higher $\delta^{44/40}Ca$ values than in the overlying seawater. The fractionation of calcium isotopes is thought to be the expression of a kinetic isotope effect, based on both experimental and theoretical constraints (Fantle and DePaolo, 2007; Tang et al., 2008; DePaolo, 2011; Nielsen et al., 2012). Aqueous diffusion of calcium within the pore fluid profile generates negligible isotope fractionation (Bourg et al., 2010). In the non-steady-state conditions captured at 940GC and 1520GC, precipitation at the SMTZ is essentially occurring within a closed system, consuming only the available reactant within the pore fluids as the SMTZ migrates towards the surface (see Fig. 5). Diffusion of calcium from the overlying seawater has no influence below the kinks in the pore fluid profiles, below which calcium is being consumed into carbonate minerals. Below the SMTZ, calcium concentrations and isotope ratios are relatively constant (Fig. 3), suggesting that no further net reaction is occurring.

The extent of back reaction between the authigenic carbonate minerals and the pore fluids is unknown, such that only the apparent fractionation associated with the net forward (attachment) and backward (detachment) reactions can be constrained. The over-saturated conditions (see sec-

tion 4.3) and the rapid decrease in calcium concentrations at the SMTZ show that the forward reaction is more important, but the balance between the net and gross precipitation rates cannot be further quantified in this setting. If isotopic exchange or re-equilibration with the authigenic carbonate minerals is important, calcium isotope ratios in the pore fluids would be lower than for a unidirectional reaction (e.g. Fantle and DePaolo (2007); Jacobson and Holmden (2008); Teichert et al. (2009)), and the apparent fractionations derived below would be smaller than (i.e. closer to equilibrium than) the fractionation associated with the forward precipitation reaction only. However, in carbonate-rich marine sediments, calcium isotopic equilibrium with sedimentary carbonate minerals is only achieved on a million-year timescale (Fantle and DePaolo, 2007), suggesting that the young Holocene cores sampled here with minor carbonate mineral components would not have experienced significant re-equilibration. Within these constraints, the pore fluids at 940GC and 1520GC can be used to estimate the apparent fractionation factor using a Rayleigh distillation model:

$$\frac{R_f}{R_0} = f^{(\alpha-1)}$$

where R_f is the calcium isotope ratio ($^{44}Ca/^{40}Ca$) of the distilled pore fluid, R_0 is the calcium isotope ratio of the initial pore fluid (assumed to be equal to the ratio in seawater, which is consistent with the measured values in the shallowest parts of the profiles, see Fig. 3), f is the fraction of calcium removed (relative to the concentration in seawater), and α is the net calcium isotope fractionation factor ($\alpha = R_{\text{carbonate}}/R_{\text{fluid}}$).

Previous studies have suggested that Rayleigh distillation could explain the variation observed in carbonate mineral deposits associated with methane hydrates and methane seeps (Teichert et al., 2005; Wang et al., 2012), but these inferences were made in the absence of measured pore fluid compositions and required assuming a constant calcium isotope fractionation factor determined under very different environmental conditions. For example, a range of $\delta^{44/40}Ca$ values (-1.4 to $-0.7‰$, converted to the seawater scale) was observed in aragonite precipitates in direct association with gas hydrates (Teichert et al., 2005). However, the observed range could equally be

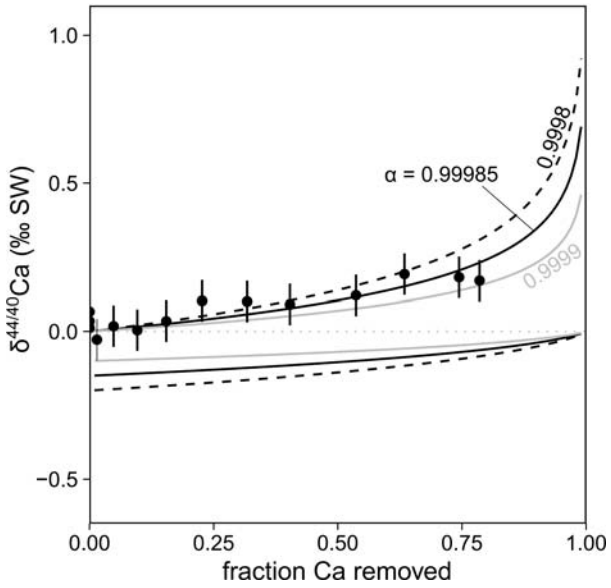

Figure 7: Rayleigh distillation model applied to pore fluid data from 940GC. Upper curves show pore fluid composition (best fit $\alpha = 0.99985$); lower curves show the integrated product (authigenic carbonate minerals). Error bars represent 1σ analytical error.

explained by variability in the fractionation factor. In a separate organic-rich sedimentary environment bearing authigenic high-Mg calcite nodules with an apparent fractionation factor of α = 0.9994–0.9992, Rayleigh distillation was expected but not observed in the pore fluids, possibly because of overprinting effects from other sedimentary processes (Teichert et al., 2009). Compared to these previous approaches, the high-resolution sampling of pore fluids at sites 940GC and 1520GC under the special conditions of rapid, non-steady-state authigenic carbonate precipitation provides an opportunity to observe this mechanism at work and resolve the magnitude of calcium isotope fractionation at these locations.

At 940GC, pore fluids are only slightly enriched in the heavier isotopes of calcium despite the substantial decrease in calcium concentration. This relationship defines a best-fit apparent fractionation factor of $\alpha = 0.99985$ (Fig. 7). For a similar change in calcium concentration, the pore fluids at 1520GC have much higher $\delta^{44/40}$Ca values, with a best fit of $\alpha = 0.9996$ (Fig. 8). The different magnitudes of the apparent fractionation factors between fluid and precipitate expressed at these sites may be caused by different precipitation rates related to the methane fluxes and also expressed in the abruptness of the concentration gradients in the pore fluid profiles (see section

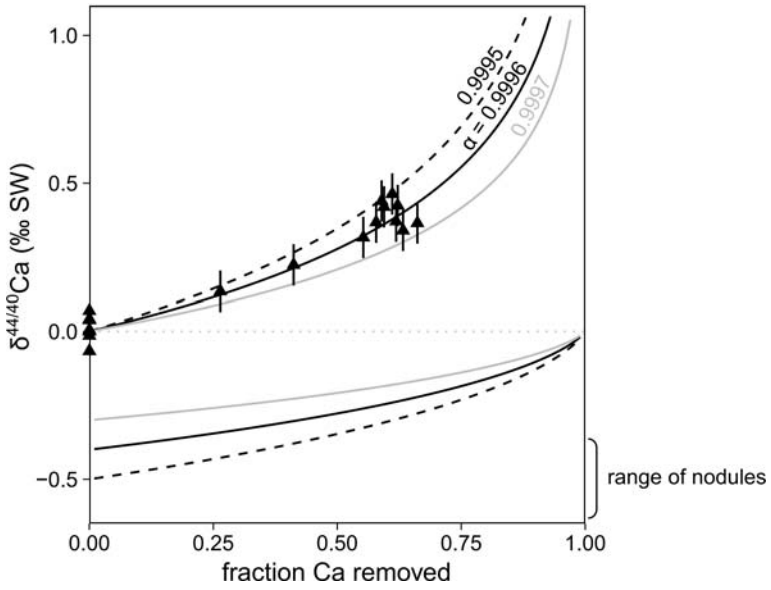

Figure 8: Rayleigh distillation model applied to pore fluid data from 1520GC. Upper curves show pore fluid composition (best fit $\alpha = 0.9996$); lower curves show the integrated product (authigenic carbonate minerals). Error bars represent 1σ analytical error.

4.3 below). Given the location of active methane seepage atop the seafloor mound (Fig. 1), this relationship is consistent with the greater distance between core 940GC and the top of the mound compared to 1520GC yielding a lower methane flux, lower precipitation rates, and smaller calcium isotope fractionation.

4.3 Relating calcium isotope fractionation to precipitation rate

Although the pore fluid profiles at these sites are presently out of steady state, the gradients preserved within specific intervals can be interpreted to estimate precipitation rates at the current locations of the SMTZ. The calcium concentration gradients below the kinks in the profiles are used to quantify the flux of calcium per unit surface area into the SMTZ following Fick's first law of diffusion for a 1D system:

$$F = -D\frac{dC}{dz} \tag{1}$$

where F is the downward calcium flux, D is the apparent diffusivity ($D = D_0/\theta^2$, where D_0 is

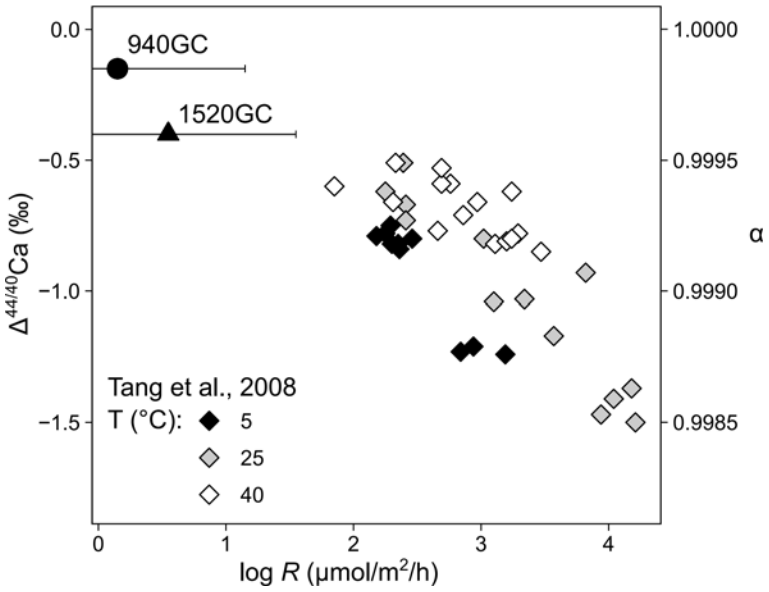

Figure 9: Comparison of calcite precipitation rates (R, per unit reactive surface area) and isotopic fractionation between calcite and aqueous fluid ($\Delta^{44/40}$Ca, α) from sites in this study and laboratory experimental data (Tang et al., 2008). For sites in this study, isotopic fractionations are calculated from a Rayleigh distillation model (section 4.2, Fig. 7,8); precipitation rates are estimated from calcium fluxes scaled to estimates of reactive surface area at the SMTZ interface at a temperature of 0 °C, with uncertainty of approximately an order of magnitude in either direction.

the estimated infinite-dilution diffusion coefficient and θ is tortuosity), and C is the concentration with z positive downwards (Boudreau, 1997). Tortuosity is estimated from porosity (ϕ) by the relation $\theta^2 = 1 - \ln(\phi^2)$. Assuming a temperature of 0 °C and $\phi = 0.7$ for conditions in the Storfjordrenna region (Hong et al., 2017), D is estimated to be 7.6×10^{-7} m^2/h. For 940GC, where a decrease in calcium concentrations of 7 mM occurs over approximately 1.5 m above the SMTZ, the flux of calcium into the SMTZ is estimated to be 3.5 μmol/m^2/h. For 1520GC, where a similar decrease occurs over 0.6 m, the flux is estimated to be 8.8 μmol/m^2/h per unit seafloor area.

Relating these calcium fluxes to estimated precipitation rates of calcium carbonate per unit reactive surface area in the natural environment requires several assumptions and rough estimates. Calcium carbonate precipitation is assumed to occur at a theoretical planar interface at the SMTZ, driven by AOM. A common approach for estimating reactive surface area for a given volume of sediment, when not measured by gas adsorption methods, for example, uses the geometrical sur-

face area (a function of grain size and shape) scaled by a roughness factor and a surface reactivity factor (Beckingham et al., 2016). Adapting this approach to the methane seep sites, where the volume of sediment involved in the reaction is undefined, the reactive surface area is taken to be the geometrical estimate of a subsurface horizontal plane (equal to the seafloor surface area used in the flux calculation above) multiplied by these two scaling factors. General values used for the roughness factor for fine-grained sediments are 10 and 160 (Zerai et al., 2006; Maher et al., 2009), while the surface reactivity factor has broad uncertainty and is estimated to be between 0.1 and 0.001 (Beckingham et al., 2016). Taking the geometric means of these ranges, the combined scaling factors yield a factor of 0.4 to convert calcium fluxes at the seafloor to calcium carbonate precipitation rates on available mineral surface area at the SMTZ. This calculation yields precipitation rates, R, per unit reactive surface area of 1.4 μmol/m^2/h at 940GC and 3.5 μmol/m^2/h at 1520GC. Uncertainties on estimating reactive surface area should be considered to be an order of magnitude in either direction, noting also that this method does not capture the lateral variability, possibly driven by nucleation kinetics, that must exist for growth of nodules rather than continuous horizons of authigenic carbonate.

These estimated precipitation rates of calcium carbonate within the present-day SMTZ are one to three orders of magnitude lower than precipitation rates achieved in the laboratory experiments of Tang et al. (2008) (Fig. 9). With the fractionation factors assessed from the pore fluid profiles of calcium isotope ratios (Figs. 7 and 8), sites 1520GC and 940GC continue the trend observed for experimentally grown calcite with greater isotopic fractionation at higher precipitation rates and smaller fractionation at slower rates. Calcium carbonate saturation is not directly comparable between the experimental and environmental settings: the saturation index ($SI_{calcite} = \log(IAP/K_{sp,calcite})$, where IAP is the ion activity product and K_{sp} is the thermodynamic solubility product) was between 0.51 and 1.23 in the experiments of Tang et al. (2008) whereas it is estimated to be 1.35 within the SMTZ at the methane seep sites, based on results from a comprehensive pore-fluid chemistry model for a core site atop the mound a few hundred meters from 940GC and 1520GC (Fig. 1) and with similar pore fluid profiles (911GC in Hong et al., 2017).

However, these methane seep sites are one of the first natural environments where the active relationship between inorganic calcite precipitation rate and calcium isotope fractionation can be quantified at conditions far enough from equilibrium to impart measurable isotopic fractionation. These results may in turn be used to help refine the parameters of theoretical models of isotopic fractionation during calcite precipitation (e.g. DePaolo, 2011; Nielsen et al., 2012). For example, the equilibrium fractionation for infinitely low precipitation rates must be closer to 1 than $\alpha = 0.99985$, based on the observations from 940GC. Notably, there appears to be less isotope fractionation at the methane seep sites than at near-equilibrium conditions where recrystallizing carbonate sediments within a deep drillcore were inferred to express $\alpha = 0.9995$ (Bradbury and Turchyn, 2018). This suggests that different settings may express different relationships between precipitation rate and calcium isotope fractionation, potentially reflecting the importance of other fluid properties, environmental conditions, or mineral surface parameters. Differences in the direction of the relationship shown in Fig. 9 have also been observed under different experimental conditions (Lemarchand et al., 2004; AlKhatib and Eisenhauer, 2017), showing less isotopic fractionation at higher precipitation rates. It has been suggested that an extremely ammonium-rich solution matrix could have changed the complexing behavior and desolvation kinetics, and therefore isotopic fractionation, of calcium ions in those experiments (AlKhatib and Eisenhauer, 2017), but further investigation is needed to fully understand the parameters that are important for shaping the relationship between calcium isotope fractionation and precipitation rate in natural environments.

4.4 Interpreting carbonate nodule geochemistry

Despite the different timescales reflected by the pore fluids (reactions occurring presently within the sediment column, not in steady-state) and the carbonate nodules (conditions integrated over longer periods of time at the past locations of the SMTZ), a comparison of their geochemistry provides additional constraints on the evolution of the methane seep system. The geochemical homogeneity within subsamples of a nodule (Fig. 4) indicates that entire nodules grew under relatively stable ambient pore fluid conditions; differences among the individual nodules show that

those conditions changed over time. This observation supports the idea that variability in nodule $\delta^{13}C$ values is related to different proportions of DIC derived from the two dominant sources, methane oxidation and diffused or buried seawater, as opposed to carbonate precipitation at depths outside of the SMTZ, which would be expected to generate spatial heterogeneity in $\delta^{13}C$ values. These proportions are controlled by the methane flux, which will establish the SMTZ (where nodules will grow) at the depth where sufficient sulfate for AOM is supplied by diffusion. The rate of AOM will in turn influence the rate of authigenic carbonate precipitation.

The nodules measured at 1520GC have $\delta^{44/40}Ca$ values lower than would be expected given the fractionation factors expressed in modern pore fluid profiles (Fig. 8). The fraction of calcium consumed during the steady-state, open-system precipitation of the nodules is unknown, preventing a precise estimate of the isotopic fractionation factor, but the average $\delta^{44/40}Ca$ values for each nodule of -0.36 to $-0.63‰$ define the maximum possible values for α (corresponding to small f) of 0.99964 to 0.99937, with lower values likely. This difference suggests that the nodules grew at faster precipitation rates than those supported by the present diffusive flux of calcium, corresponding to higher methane fluxes and a shallower SMTZ. The nodules recovered at shallower depths than the modern SMTZ are consistent with this interpretation (see Fig. 6), although their presence could also be explained by surface erosion. Although the history of methane seepage in this region cannot be fully reconstructed, it is possible that pulses of higher methane flux capable of supporting the growth of authigenic carbonate nodules were episodic, which would also be consistent with the presence of nodules at discontinuous intervals throughout the core. At Hydrate Ridge (offshore Oregon, USA), variable $\delta^{44/40}Ca$ values reported in carbonate crusts directly associated with methane hydrate deposits (Teichert et al., 2005) may similarly be caused by different fractionation factors related to the rate of methane oxidation. This interpretation differs from the previous hypothesis for those deposits (Teichert et al., 2005) that pore fluids in that setting evolved towards very high $\delta^{44/40}Ca$ values (up to $0.8‰$ heavier than seawater), which would be challenging to maintain with the mass balance requirement of supplying calcium by diffusion for the carbonate crusts. These two possibilities, rate-dependent isotope fractionation or ^{44}Ca-enriched pore fluids,

could potentially be tested with trace element analyses of the crusts.

For the authigenic carbonates at 1520GC, variable precipitation rates, as interpreted from their $\delta^{44/40}$Ca values, also correlate with variations in trace element composition and mineralogy. Faster rates (lower $\delta^{44/40}$Ca values) yield lower Mg/Ca ratios and higher Sr/Ca ratios (Fig. 4), and also correspond to higher proportions of aragonite. Contributions from aluminosilicates or other non-carbonate phases appear to be negligible based on the lack of correlation between measured Mg/Ca and Al, Li, or Mn concentrations, for example (Table 3). The observed relationships within the carbonate nodules likely include the combined effects of three factors, all of which are potentially functions of precipitation rate: 1) changing distribution coefficients for a given carbonate polymorph, 2) precipitation of a mix of Mg-calcite and aragonite, and 3) changing pore fluid Mg/Ca and Sr/Ca within the SMTZ. The importance of changing distribution coefficients for Mg-calcite is suggested by the correlations between Mg/Ca, Sr/Ca, and $\delta^{44/40}$Ca values where Mg-calcite is the dominant authigenic phase (< 1% or no detectable aragonite). In contrast, the composition of the subsample with the highest fraction of aragonite measured is most likely the result of its mineralogy, as is much of the variability observed in seafloor methane-derived carbonate crusts analyzed from the Barents and North Seas (Thiagarajan et al., 2020) (Fig. 4). These observations are consistent with models that suggest connections between calcium isotope fractionation and trace element distributions are linked to the kinetics of ion desolvation and attachment (Gussone et al., 2005; Tang et al., 2008; DePaolo, 2011; Nielsen et al., 2012). However, it is not clear how important these effects are generally for other (e.g. biogenic) carbonates, since the variations in precipitation rates for these inorganic methane-seep carbonates are externally controlled and more extreme compared to many other settings of carbonate precipitation. Changes in pore fluid Mg/Ca and Sr/Ca, which are not known for the time intervals when the nodules grew, may also contribute to some of the variability in the nodules. In the present day SMTZ at 1520GC, the elevated molar Mg/Ca ratio of 13 (2.5 times the ratio in seawater) and Sr/Ca ratio of 0.016 (2 times the ratio in seawater) are primarily driven by the drawdown of calcium, with much smaller relative decreases in magnesium and strontium concentrations (Fig. 3). Variation in these ratios over time during

periods of nodule growth cannot be ruled out, but their similarity at the two sites, 940GC and 1520GC, despite different methane fluxes and precipitation rates, suggests that they may not be the dominant contribution to trace element variability of the authigenic nodules.

Precipitation rate may also partly determine which polymorph of calcium carbonate forms, which can explain some fraction of the geochemical variability in the 1520GC nodules. Both aragonite and Mg-calcite are common authigenic precipitates at methane seeps. A variety of physicochemical parameters influence which mineral phase forms, with methane flux and ambient sulfate concentrations exerting a strong control (Greinert et al., 2001; Peckmann et al., 2001). Aragonite precipitation typically occurs under high methane flux conditions with a shallow SMTZ near the sediment-water interface where sulfate is abundant, which can result in carbonate-cemented seafloor crusts where aragonite forms fibrous cement and/or fills cavities (Crémière et al., 2016). On the other hand, Mg-calcite (up to 20 mol% Mg) forms under lower methane flux when the SMTZ is within subsurface sediments and porewater sulfate is relatively low (Naehr et al., 2007). Spotty cementation of detrital sediments by micritic Mg-calcite results in formation of nodules like those seen at the Storfjordrenna sites. In the Barents and North Seas, carbonate crusts containing both aragonite and Mg-calcite were recovered from methane seeps, with petrographic evidence that the aragonite formed at higher methane fluxes and precipitation rates (Thiagarajan et al., 2020). For those crusts, rapid precipitation rates were also required to explain disequilibrium isotope effects observed in carbonate clumped isotope measurements for certain aragonite phases (Thiagarajan et al., 2020). The nodules from 1520GC overlap with a limited fraction of the compositional variability observed in the Barents and North Sea seep carbonates (Fig. 4), indicating consistent mineralogical and kinetic effects shared across these samples.

5 Conclusions

Previous experimental and theoretical work has shown that calcium isotope fractionation in calcium carbonate minerals is a function of mineralogy and precipitation rate. This study demon-

strates the expression of these relationships in a natural setting where authigenic carbonate is precipitating at a methane seep site in the northern Barents Sea near Svalbard. This setting allows for the quantification of carbonate precipitation rates driven by the anaerobic oxidation of methane within the sediment column through analysis of pore fluid geochemical profiles. The pore fluid profiles show elevated calcium isotope ratios from precipitation of authigenic carbonate with calcium isotope fractionation factors of α = 0.9996 to 0.99985, a smaller magnitude of calcium isotope fractionation than expressed in typical marine carbonates. The range of observed fractionations reflects different rates of precipitation driven by variable methane fluxes and rates of anaerobic oxidation of methane. The variation in precipitation rate also affects the trace element composition of the carbonates (Mg/Ca and Sr/Ca ratios), as well as the polymorph of calcium carbonate (Mg-calcite versus aragonite). This system of inorganic carbonate precipitation provides the necessary constraints for distinguishing multiple controls on geochemical variability and confirming mechanisms of calcium isotope fractionation in these mineral archives.

Acknowledgments

The authors would like to acknowledge the captains and crews onboard R/V Helmer Hanssen for cruises CAGE15-2 and CAGE15-6 and thank the chief scientists Dr. Giuliana Panieri (CAGE15-2) and Dr. Jürgen Mienert (CAGE15-6). This work was supported by the Research Council of Norway through its Centres of Excellence funding scheme (project number 223259) and NORCRUST (project number 255150).

References

AlKhatib, M. and Eisenhauer, A. (2017) Calcium and strontium isotope fractionation in aqueous solutions as a function of temperature and reaction rate; I. Calcite. *Geochimica et Cosmochimica Acta* 209:296–319.

510 Andersen, E. S., Dokken, T. M., Elverhøi, A., Solheim, A., and Fossen, I. (1996) Late Quaternary
511 sedimentation and glacial history of the western Svalbard continental margin. *Marine Geology*
512 133:123–156.

513 Beckingham, L. E., Mitnick, E. H., Steefel, C. I., Zhang, S., Voltolini, M., Swift, A. M., Yang,
514 L., Cole, D. R., Sheets, J. M., Ajo-Franklin, J. B., DePaolo, D. J., Mito, S., and Xue, Z. (2016)
515 Evaluation of mineral reactive surface area estimates for prediction of reactivity of a multi-
516 mineral sediment. *Geochimica et Cosmochimica Acta* 188:310–329.

517 Bischoff, W. D., Bishop, F. C., and Mackenzie, F. T. (1983) Biogenically produced magnesian
518 calcite: Inhomogeneities in chemical and physical properties; comparison with synthetic phases.
519 *American Mineralogist* 68:1183–1188.

520 Blättler, C. L., Henderson, G. M., and Jenkyns, H. C. (2012) Explaining the Phanerozoic Ca
521 isotope history of seawater. *Geology* 40:843–846.

522 Blättler, C. L. and Higgins, J. A. (2017) Testing Urey's carbonate–silicate cycle using the calcium
523 isotopic composition of sedimentary carbonates. *Earth and Planetary Science Letters* 479:241–
524 251.

525 Blättler, C. L., Higgins, J. A., and Swart, P. K. (2019) Advected glacial seawater preserved in the
526 subsurface of the Maldives carbonate edifice. *Geochimica et Cosmochimica Acta* 257:80–95.

527 Boudreau, B. P. (1997) *Diagenetic models and their implementation; modelling transport and*
528 *reactions in aquatic sediments*. Springer, Berlin.

529 Bourg, I. C., Richter, F. M., Christensen, J. N., and Sposito, G. (2010) Isotopic mass dependence of
530 metal cation diffusion coefficients in liquid water. *Geochimica et Cosmochimica Acta* 74:2249–
531 2256.

532 Bradbury, H. J. and Turchyn, A. V. (2018) Calcium isotope fractionation in sedimentary pore fluids

from ODP Leg 175: Resolving carbonate recrystallization. *Geochimica et Cosmochimica Acta* 236:121–139.

Crémière, A., Lepland, A., Chand, S., Sahy, D., Condon, D. J., Noble, S. R., Martma, T., Thorsnes, T., Sauer, S., and Brunstad, H. (2016) Timescales of methane seepage on the Norwegian margin following collapse of the Scandinavian Ice Sheet. *Nature Communications* 7:11509.

DePaolo, D. J. (2011) Surface kinetic model for isotopic and trace element fractionation during precipitation of calcite from aqueous solutions. *Geochimica et Cosmochimica Acta* 75:1039–1056.

Fantle, M. S. and DePaolo, D. J. (2007) Ca isotopes in carbonate sediment and pore fluid from ODP Site 807A: The Ca^{2+}(aq)–calcite equilibrium fractionation factor and calcite recrystallization rates in Pleistocene sediments. *Geochimica et Cosmochimica Acta* 71:2524–2546.

Fantle, M. S. and Tipper, E. T. (2014) Calcium isotopes in the global biogeochemical Ca cycle: Implications for development of a Ca isotope proxy. *Earth-Science Reviews* 129:148–177. doi:10.1016/j.earscirev.2013.10.004.

Greinert, J., Bohrmann, G., and Suess, E. (2001) Gas hydrate-associated carbonates and methane-venting at Hydrate Ridge: classification, distribution and origin of authigenic lithologies. *Geophysical Monograph-American Geophysical Union* 124:99–114.

Gussone, N., Böhm, F., Eisenhauer, A., Dietzel, M., Heuser, A., Teichert, B. M. A., Reitner, J., Wörheide, G., and Dullo, W.-C. (2005) Calcium isotope fractionation in calcite and aragonite. *Geochimica et Cosmochimica Acta* 69:4485–4494.

Gussone, N., Eisenhauer, A., Heuser, A., Dietzel, M., Bock, B., Böhm, F., Spero, H. J., Lea, D. W., Bijma, J., and Nägler, T. F. (2003) Model for kinetic effects on calcium isotope fractionation (δ^{44}Ca) in inorganic aragonite and cultured planktonic foraminifera. *Geochimica et Cosmochimica Acta* 67:1375–1382.

Gussone, N., Hönisch, B., Heuser, A., Eisenhauer, A., Spindler, M., and Hemleben, C. (2009) A critical evaluation of calcium isotope ratios in tests of planktonic foraminifers. *Geochimica et Cosmochimica Acta* 73:7241–7255.

Heuser, A. and Eisenhauer, A. (2008) The calcium isotope composition ($\delta^{44/40}$Ca) of NIST SRM 915b and NIST SRM 1486. *Geostandards and Geoanalytical Research* 32:311–315.

Heuser, A., Schmitt, A.-D., Gussone, N., and Wombacher, F. (2016) *Analytical Methods*, pages 23–73. Springer Berlin Heidelberg, Berlin, Heidelberg.

Hippler, D., Schmitt, A.-D., Gussone, N., Heuser, A., Stille, P., Eisenhauer, A., and Nägler, T. F. (2003) Calcium isotopic composition of various reference materials and seawater. *Geostandards Newsletter* 27:13–19.

Hong, W.-L., Torres, M. E., Carroll, J., Crémière, A., Panieri, G., Yao, H., and Serov, P. (2017) Seepage from an arctic shallow marine gas hydrate reservoir is insensitive to momentary ocean warming. *Nature Communications* 8:15745.

Hong, W.-L., Torres, M. E., Portnov, A., Waage, M., Haley, B., and Lepland, A. (2018) Variations in gas and water pulses at an Arctic seep: fluid sources and methane transport. *Geophysical Research Letters* 45:4153–4162.

Jacobson, A. D., Andrews, M. G., Lehn, G. O., and Holmden, C. (2015) Silicate versus carbonate weathering in Iceland: New insights from Ca isotopes. *Earth and Planetary Science Letters* 416:132–142.

Jacobson, A. D. and Holmden, C. (2008) δ^{44}Ca evolution in a carbonate aquifer and its bearing on the equilibrium isotope fractionation factor for calcite. *Earth and Planetary Science Letters* 270:349–353.

Lemarchand, D., Wasserburg, G. J., and Papanastassiou, D. A. (2004) Rate-controlled calcium

isotope fractionation in synthetic calcite. *Geochimica et Cosmochimica Acta* 68:4665–4678. doi:10.1016/ j.gca.2004.05.029.

Maher, K., Steefel, C. I., White, A. F., and Stonestrom, D. A. (2009) The role of reaction affinity and secondary minerals in regulating chemical weathering rates at the Santa Cruz Soil Chronosequence, California. *Geochimica et Cosmochimica Acta* 73:2804–2831.

Naehr, T. H., Eichhubl, P., Orphan, V. J., Hovland, M., Paull, C. K., Ussler III, W., Lorenson, T. D., and Greene, H. G. (2007) Authigenic carbonate formation at hydrocarbon seeps in continental margin sediments: A comparative study. *Deep Sea Research Part II: Topical Studies in Oceanography* 54:1268–1291.

Nielsen, L. C., DePaolo, D. J., and De Yoreo, J. J. (2012) Self-consistent ion-by-ion growth model for kinetic isotopic fractionation during calcite precipitation. *Geochimica et Cosmochimica Acta* 86:166–181.

Peckmann, J., Reimer, A., Luth, U., Luth, C., Hansen, B. T., Heinicke, C., Hoefs, J., and Reitner, J. (2001) Methane-derived carbonates and authigenic pyrite from the northwestern Black Sea. *Marine geology* 177:129–150.

Romanek, C. S., Grossman, E. L., and Morse, J. W. (1992) Carbon isotopic fractionation in synthetic aragonite and calcite: effects of temperature and precipitation rate. *Geochimica et Cosmochimica Acta* 56:419–430.

Skulan, J., DePaolo, D. J., and Owens, T. L. (1997) Biological control of calcium isotopic abundances in the global calcium cycle. *Geochimica et Cosmochimica Acta* 61(12):2505–2510.

Steiner, Z., Lazar, B., Erez, J., and Turchyn, A. V. (2018) Comparing Rhizon samplers and centrifugation for pore-water separation in studies of the marine carbonate system in sediments. *Limnology and Oceanography: Methods* 16:828–839.

603 Tada, R., Murray, R. W., Alvarez Zarikian, C. A., and the Expedition 346 Scientists (2015) Site
604 U1425. In *Proceedings of the Integrated Ocean Drilling Program*, volume 346. International
605 Ocean Discovery Program, College Station, TX.

606 Tang, J., Dietzel, M., Böhm, F., Köhler, S. J., and Eisenhauer, A. (2008) Sr^{2+}/Ca^{2+} and $^{44}Ca/^{40}Ca$
607 fractionation during inorganic calcite formation: II. Ca isotopes. *Geochimica et Cosmochimica*
608 *Acta* 72:3733–3745.

609 Tang, J., Niedermayr, A., Köhler, S. J., Böhm, F., Kısakürek, B., Eisenhauer, A., and Dietzel, M.
610 (2012) Sr^{2+}/Ca^{2+} and $^{44}Ca/^{40}Ca$ fractionation during inorganic calcite formation: III. Impact of
611 salinity/ionic strength. *Geochimica et Cosmochimica Acta* 77:432–443.

612 Teichert, B. M., Gussone, N., Eisenhauer, A., and Bohrmann, G. (2005) Clathrites: archives of
613 near-seafloor pore-fluid evolution ($\delta^{44/40}$Ca, δ^{13}C, δ^{18}O) in gas hydrate environments. *Geology*
614 33:213–216.

615 Teichert, B. M., Gussone, N., and Torres, M. E. (2009) Controls on calcium isotope fractionation
616 in sedimentary porewaters. *Earth and Planetary Science Letters* 279:373–382.

617 Thiagarajan, N., Crémière, A., Blättler, C., Lepland, A., Kirsimäe, K., Higgins, J. A., Brunstad,
618 H., and Eiler, J. (2020) Stable and clumped isotope characterization of authigenic carbonates in
619 methane cold seep environments. *Geochimica et Cosmochimica Acta* 279:204–219.

620 Torres, M. E., Mix, A. C., and Rugh, W. D. (2005) Precise δ^{13}C analysis of dissolved inorganic
621 carbon in natural waters using automated headspace sampling and continuous-flow mass spec-
622 trometry. *Limnology and Oceanography: Methods* 3:349–360.

623 Wang, S., Yan, W., Magalhães, H. V., Chen, Z., Pinheiro, M. L., and Gussone, N. (2012) Calcium
624 isotope fractionation and its controlling factors over authigenic carbonates in the cold seeps of
625 the northern South China Sea. *Chinese Science Bulletin* 57:1325–1332.

626 Wittke, A., Gussone, N., M¨ärz, C., and Teichert, B. M. A. (2020) The effect of extraction tech-
627 niques on calcium concentrations and isotope ratios of marine pore water. *Isotopes in Environ-*
628 *mental and Health Studies* 56:51–68.

629 Young, E. D., Galy, A., and Nagahara, H. (2002) Kinetic and equilibrium mass-dependent isotope
630 fractionation laws in nature and their geochemical and cosmochemical significance. *Geochimica*
631 *et Cosmochimica Acta* 66:1095–1104.

632 Zerai, B., Saylor, B. Z., and Matisoff, G. (2006) Computer simulation of CO_2 trapped through
633 mineral precipitation in the Rose Run Sandstone, Ohio. *Applied Geochemistry* 21(2):223 – 240.

634 Zhang, F., Xu, H., Konishi, H., and Roden, E. E. (2010) A relationship between d_{104} value and
635 composition in the calcite-disordered dolomite solid-solution series. *American Mineralogist*
636 95:1650–1656.

Small calcium isotope fractionation at slow precipitation rates in methane seep authigenic carbonates

Clara L. Blättler*[a,b], Wei-Li Hong[c,d], Kalle Kirsimäe[e], John A. Higgins[b], and Aivo Lepland[c,d,e]

[a]Department of the Geophysical Sciences, University of Chicago, Chicago, IL, USA.

[b]Department of Geosciences, Princeton University, Princeton, NJ, USA.

[c]Geological Survey of Norway, Trondheim, Norway.

[d]Centre for Arctic Gas Hydrate, Environment and Climate, UiT The Arctic University of Norway, Tromsø, Norway.

[e]Department of Geology, University of Tartu, Tartu, Estonia.

*Corresponding author: cblattler@uchicago.edu

Abstract

Natural calcium carbonate minerals express a range of calcium isotope fractionations, with the precipitated mineral typically enriched in the lighter isotopes of calcium relative to source fluids. Experimental and theoretical evidence shows a strong dependence on precipitation rate, although this relationship has not been well quantified over the range of precipitation rates observed in natural settings. Endmember cases show that average marine carbonate precipitation expresses a large fractionation ($\delta^{44/40}$Ca values lower than seawater by approximately 1‰), while diagenetic carbonate phases assumed to have precipitated or recrystallized at very slow rates show negligible fractionation. The limited examples of quantified precipitation rates in natural settings with measurable, non-zero fractionation represents a barrier for applying mechanistic models of calcium isotope fractionation to geological applications. This study examines a methane seep system in the northern Barents Sea south of Svalbard where authigenic carbonate minerals are precipitating, driven by anaerobic oxidation of methane, and where the apparent calcium isotope fractionation factor and precipitation rate can be constrained by measuring properties of the pore fluids. Pore fluid profiles are analyzed in two shallow cores, and authigenic carbonate nodules are analyzed in one of these cores. The pore fluid profiles point to a transitional, non-steady state which approximates a closed system, where the elevation of pore fluid calcium isotope ratios through carbonate precipitation can be modeled as a Rayleigh distillation system. The apparent fractionation factors for ^{44}Ca/^{40}Ca ratios at these sites are α = 0.99985 and 0.9996, although the carbonate nodules suggest a different calcium isotope fractionation factor may have been expressed under past conditions. Precipitation rates at the two sites are estimated to be 1.4 and 3.5 μmol/m^2/h, intermediate between those of typical laboratory experiments and the much slower rates of marine diagenesis. Trace element analyses of the nodules (Mg/Ca and Sr/Ca ratios) suggest that both precipitation rate and mineralogy affect nodule composition. These results provide new constraints for the relationship between precipitation rate and calcium isotope fractionation and can inform modeling efforts leading towards mechanistic understanding of calcium isotope fractionation and trace element distributions in carbonate minerals.

1 Introduction

Natural calcium carbonate minerals show a wide spread of calcium isotope ratios, with $\delta^{44/40}Ca$ values of modern marine carbonates generally showing isotope fractionations between -1.8 to $-0.8‰$ from seawater (Skulan et al., 1997; Blättler et al., 2012; Fantle and Tipper, 2014). The source of this variability is not fully understood, but two dominant factors that have been shown to affect calcium isotope fractionation in controlled precipitation experiments are the $CaCO_3$ mineral polymorph (i.e. calcite or aragonite) and precipitation rate. The mineral polymorph effect has been observed in both natural and laboratory settings (Gussone et al., 2003, 2005; Blättler et al., 2012), with aragonite expressing greater calcium isotope fractionation than calcite. However, the effect of precipitation rate derived from laboratory experiments and theoretical models (Tang et al., 2008, 2012; Nielsen et al., 2012) has been challenging to demonstrate in the natural environment. End-member cases suggest that precipitation rate does indeed affect calcium isotope fractionation in the direction predicted by experiments and theory, with biogenic carbonates expressing fractionations on the order of $-1‰$ or greater (e.g. Skulan et al., 1997; Gussone et al., 2003, 2009), yet slow, diagenetic reactions apparently producing no isotopic fractionation (Fantle and DePaolo, 2007; Jacobson and Holmden, 2008). Recently, intermediate calcium isotope fractionations have been inferred from surface deposits at cold seeps in the South China Sea (Wang et al., 2012) and from a deep drillcore site off the west coast of South Africa (Bradbury and Turchyn, 2018), although uncertainties about fluid sources, advection, and diffusion in these settings prevent direct comparison to published calibrations with precipitation rate (e.g. Tang et al., 2008). The lack of documented calcium isotope fractionation at well constrained natural precipitation rates represents a limit to understanding calcium isotope variability in ancient carbonate rocks.

This study presents calcium isotope ratios for a methane seep system off the coast of Svalbard where the fractionation factor and precipitation rate for authigenic carbonate precipitation can be constrained by measurements of pore fluid properties, and then also compared to authigenic carbonate nodules grown over previous intervals of time. Previous calcium isotope measurements of carbonates from methane-associated sedimentary systems show large variability (Teichert et al.,

2005, 2009; Wang et al., 2012; Thiagarajan et al., 2020), but these datasets are not sufficiently well characterized (e.g. limited sampling resolution, lacking paired analyses of fluid and mineral phases) to effectively determine the relative importance of changing fractionation factors, pore fluid composition, and competing reactions within the sedimentary column. Here, sampling of pore fluids on a scale of 10s of centimeters as well as carbonate nodules recovered from one of the same cores allows for the sources of calcium isotope variability to be determined and for an exploration of authigenic carbonate precipitation on two different timescales. The specific history of pore fluid evolution at these sites, which are not presently at steady state but instead represent transitional, effectively closed systems (section 4.1), provides the opportunity to quantitatively estimate precipitation rates (section 4.3). Precipitation rates for authigenic carbonate are controlled by methane seepage and its anaerobic oxidation and are found to be at least an order of magnitude lower than those achieved in laboratory experiments (Tang et al., 2008). By capturing intermediate rates between the rapid precipitation characteristic of tropical biogenic carbonates and the slower rates of near-equilibrium diagenetic reactions, this natural experiment provides a link between the rate dependencies shown in experimental and theoretical studies of calcium isotope fractionation and those recorded in environmental settings. These results may then be used to test the predictions of mechanistic models of carbonate precipitation (e.g. Fantle and DePaolo, 2007; DePaolo, 2011; Nielsen et al., 2012), leading to better strategies for interpreting and extracting useful paleoenvironmental information from calcium carbonate archives.

2 Samples and methods

2.1 Core locations

The two sediment cores studied here were recovered from 386 m water depth at a seep field in the Storfjordrenna Trough ~50 km south of Svalbard (Fig. 1). The sediments of the Svalbard shelf generally consist of glaciomarine clay and silt (Andersen et al., 1996), and measured bottom water temperatures over the past several decades are between −2 and +5 °C (Hong et al., 2017). The

Table 1: Information about gravity cores collected in 2015 (Hong et al., 2017) and analyzed in this study.

cruise	core name	core recovery	water depth	latitude	longitude
CAGE15-2	940GC	3.10 m	386 m	76.1069°N	15.9779°E
CAGE15-6	1520GC	2.90 m	386 m	76.1057°N	15.9661°E

seafloor topography in the region shows mounds hundreds of meters wide with relief up to 10 m that bear evidence for current and past methane seepage (Hong et al., 2017). Evidence for active seepage at Storfjordrenna comes from hydroacoustic flares and bubble streams, and the evolution of methane seepage and pore fluid chemistry in the region has previously been studied by analysis of multiple gravity cores (Hong et al., 2017, 2018).

Gravity cores 940GC and 1520GC were recovered during two separate cruises in 2015 (see Table 1). Although active gas escape was not observed at either core site at the time of sampling, core 1520GC contained gas hydrates, and both cores bear authigenic carbonate nodules. Two nodules were reported from 940GC at 1.28 and 1.99 mbsf, and 26 nodules were reported from 1520GC between 0.46 and 3.48 mbsf (Hong et al., 2017). A sedimentary age model for the cores was derived from two radiocarbon ages of planktic foraminifera from an adjacent core, correlated to 940GC and 1520GC through results of X-ray fluorescence (XRF) scanning. Based on this age model, the sediments in the two cores date approximately from the onset of the last deglaciation through the Holocene with approximate sedimentation rates of 0.2 mm/yr. The youngest part of the Holocene appears to be missing at core 1520GC, possibly due to erosion (Hong et al., 2017).

2.2 Sampling

Pore fluids were recovered from both cores using acid-washed Rhizon samplers inserted into the cores. Fluids were collected into 20 mL acid-washed syringes and filtered through 0.2 μm cellulose acetate filters. Aliquots for cation analysis were acidified with 10 μL of reagent grade nitric acid, and those for carbon isotope analysis were poisoned with 10 μL of $HgCl_2$. Previous work has shown that sampling pore fluids with pre-wetted Rhizons yields accurate results for major ion concentrations, including calcium (Tada et al., 2015; Steiner et al., 2018), although small, systematic

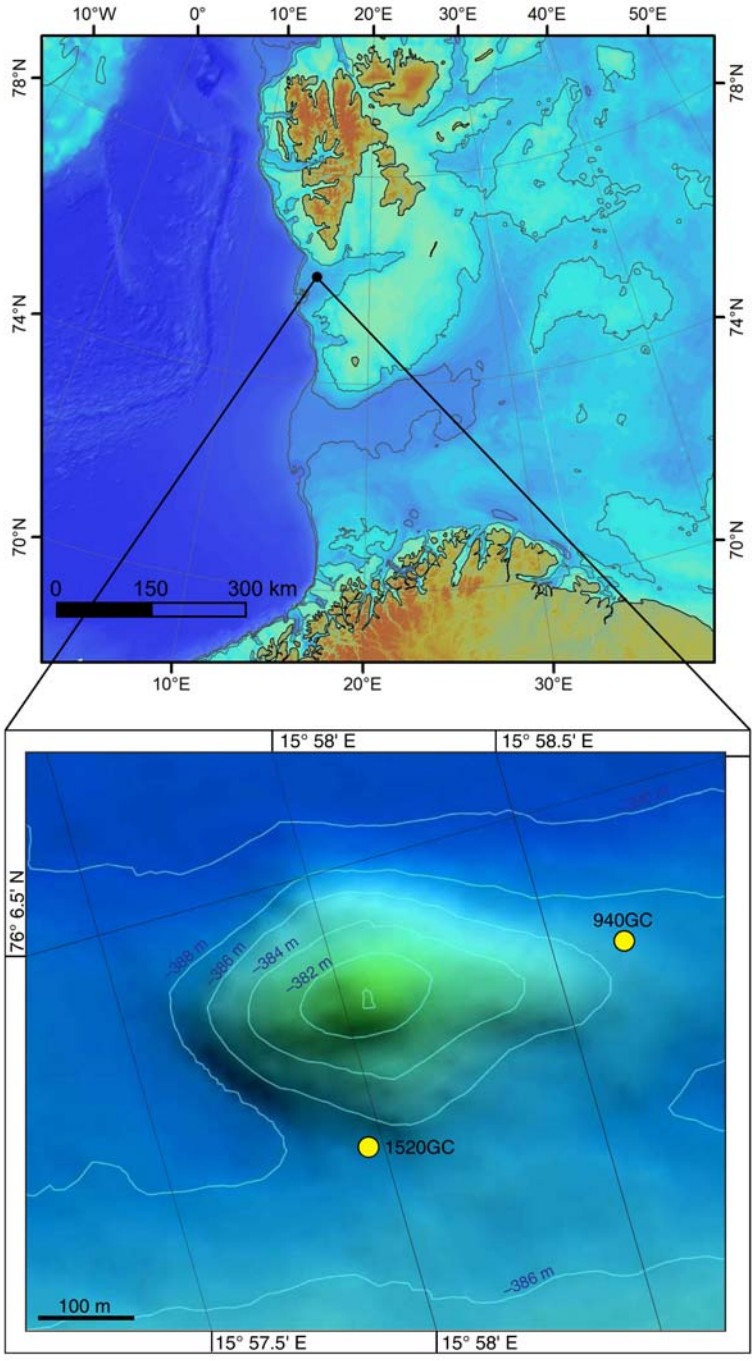

Figure 1: Regional map showing core sites on the edge of an actively discharging hydrate mound.

offsets have been observed for carbon isotope ratios (Steiner et al., 2018) and calcium isotope ratios (Wittke et al., 2020). Relative to centrifugation, pore fluids sampled with Rhizons were found to have elevated $\delta^{13}C$ values by approximately 0–1‰ (Steiner et al., 2018); relative to whole-round squeezing, Rhizon samples were found to have elevated $\delta^{44/40}Ca$ values by <0.1‰ (Wittke et al., 2020). These offsets, possibly driven by calcium carbonate precipitation and ion-exchange processes, do not affect assessments of relative changes within a pore-fluid profile, and can potentially be corrected by comparing the profile across the sediment-water interface to the composition of the bottom water (see section 3.1).

The geochemistry and mineralogy of six authigenic carbonate nodules from 1520GC were also analyzed. The six nodules, chosen from over 20 separate nodules identified in the core, were recovered between the depths of 0.52 and 3.38 mbsf. The weakly cemented nodules range in size from 0.3 to 4.0 cm, with irregular lumpy shapes (see Fig. 2). Direct radiometric dating of the carbonate minerals by U-Th isotope analysis (e.g. Crémière et al., 2016) is not possible because of abundant detrital components in the nodules contaminating the U-Th signal from the carbonate phases. Carbon isotope ratios ($\delta^{13}C$ values) of the six nodules were previously reported and range from −30.6 to −23.6‰ (Hong et al., 2017). Multiple subsamples were obtained from each nodule by drilling at different spots to obtain powders for calcium isotope analysis and quantitative mineralogical analysis by X-ray diffraction (XRD). The carbonate within nodules is mainly represented by authigenic precipitates, although a minor non-authigenic component of detrital dolomite and biogenic calcite debris (foraminifera) may also be present.

2.3 Geochemical analyses

The analysis of calcium isotope ratios for the pore fluids and carbonate nodules follows previously documented methods (Blättler and Higgins, 2017; Blättler et al., 2019). Carbonate powders were dissolved in 0.1 M acetic acid buffered with ammonium hydroxide to a pH of approximately 4.5 to minimize solubility of non-carbonate phases, then centrifuged and separated from the insoluble residue. Both pore fluids and dissolved carbonates were then prepared for isotopic analysis by sep-

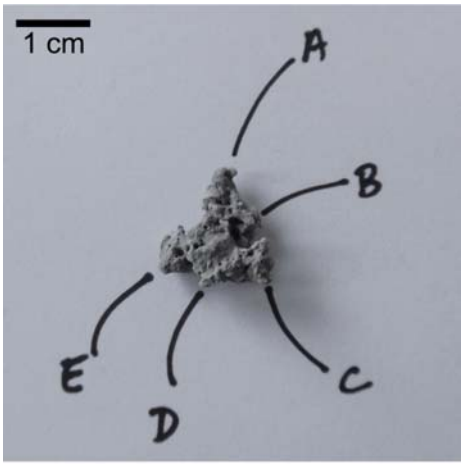

Figure 2: Carbonate nodule from 1520GC at 0.515 mbsf, showing a representative irregular shape and the locations of five subsamples (A–E) drilled for geochemical analyses.

arating calcium through automated ion chromatography. Samples were diluted with 0.2% HNO_3 to between 20 and 60 ppm Ca, and injections of 200 µL of sample were eluted through a cation-exchange column with methanesulfonic acid. Purified calcium solutions were then dried down, treated with concentrated HNO_3, dried down again, and diluted with 2% HNO_3 in preparation for analysis by multi-collector inductively coupled plasma mass spectrometry (ICP-MS). Mass spectrometric methods follow those reported in Blättler and Higgins (2017). Reported $\delta^{44/40}$Ca values are calculated from initial $\delta^{44/42}$Ca values using analyses of ^{44}Ca, ^{43}Ca, and ^{42}Ca and sample-standard bracketing with an in-house single-element ICP-MS calcium solution as the reference standard. These $\delta^{44/42}$Ca values are normalized to samples of modern seawater (SW) treated as samples and run in the same batch and then converted to $\delta^{44/40}$Ca values assuming exponential mass fractionation (Young et al., 2002) and no radiogenic ^{40}Ca excess. The long-term reproducibility of these laboratory methods for repeated analyses of carbonate minerals as well as seawater-matrix samples is identical at ±0.14‰ (2σ standard deviation), and the measured $\delta^{44/40}$Ca value of SRM915b relative to seawater is −1.15‰ (n = 199, 2σ = 0.14‰; identical within errors to reported values of −1.16 ± 0.08‰ (Heuser and Eisenhauer, 2008) and −1.13 ± 0.04‰ (Jacobson et al., 2015)). Data are reported relative to seawater (‰, or ‰ SW) and additionally presented relative to NIST SRM 915a (‰ 915a) using the published conversion: $\delta^{44/40}Ca_{915a} = \delta^{44/40}Ca_{SW} + 1.88‰$ (Hippler et al., 2003; Heuser et al., 2016).

Mineralogical and trace element analyses were also conducted on the subsamples of the carbonate nodules from 1520GC. The acetic-acid-soluble components of the samples were analyzed by ICP-MS using scandium as an internal standard. Elemental ratios relative to calcium are reported using external standards matrix-matched to a similar concentration of calcium (10 ppm). Repeat analyses of the carbonate standard NIST SRM 88b indicate analytical precision better than ± 5%. The mineralogical composition of powders from the same locations on the nodules was studied by X-ray diffractometry (XRD). The minute samples were pulverized by hand with an agate mortar and pestle under ethanol and preparations were made by dropping the sample suspension onto low-background silicon wafers. The mineralogical composition was interpreted and modeled using the Rietveld algorithm-based code Topaz by Bruker. The relative error of quantification, based on analyzing known, homogenized mixtures of rock-forming minerals, is better than 10% for major phases (>5 wt%) and better than 20% for minor phases (<5 wt%). Unit-cell parameters of calcite and Mg-calcite phases were obtained by using Rietveld structure refinement. The magnesium content ($MgCO_3$ mol%) of calcite was estimated from the unit cell *a* parameter according to Bischoff et al. (1983) and Zhang et al. (2010).

Carbon isotope measurements for dissolved inorganic carbon in the pore fluids were made in the Stable Isotope Laboratory at Oregon State University using a Finnigan GasBench-II headspace sampler with an online Finnigan DELTAplusXL gas-source isotope-ratio mass spectrometer (Torres et al., 2005). Pore fluids were sampled with a syringe and loaded into clean septum-capped vials that were then flushed with helium. The samples were acidified with phosphoric acid and the headspace gases were sampled, dried, eluted through a gas chromatography system, and fed directly into the isotope-ratio mass spectrometer. Carbon isotope ratios were normalized to multiple standards run before and after each sample and calibrated to known international standards. The average standard deviation for pore fluid $\delta^{13}C$ values measured with these methods is ± 0.04‰ (Torres et al., 2005).

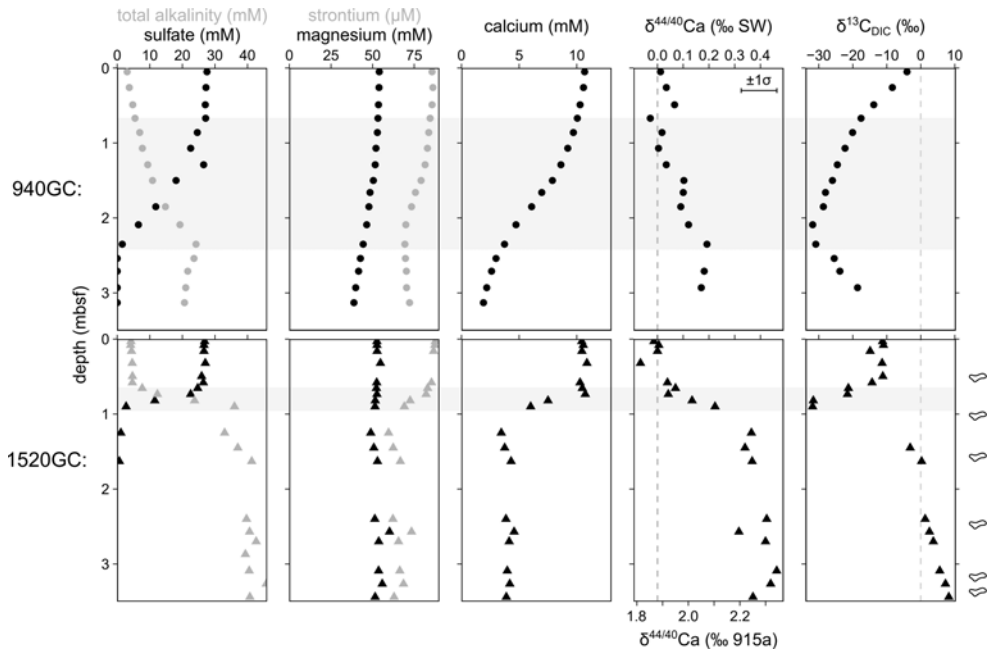

Figure 3: Pore fluid profiles from 940GC and 1520GC. Gray bands show the intervals of decreasing sulfate concentrations, including the modern sulfate–methane transition zone (SMTZ). Symbols at right show depths of nodules analyzed in this study. Calcium isotope ratios ($\delta^{44/40}$Ca values) and carbon isotope ratios (δ^{13}C values) are from this study; concentration data were previously reported in Hong et al. (2017) and Hong et al. (2018).

3 Results

3.1 Pore fluids

Pore fluid profiles for cores 940GC and 1520GC show many similar features, but differ in the depths at which geochemical changes occur as well as the extent and abruptness of these changes (Fig. 3, Table 2). In core 940GC, sulfate concentrations drop to zero between 0.8 and 2.5 mbsf (meters below sea floor) while total alkalinity rises to 24 mM. Magnesium and strontium concentrations decrease to 40 mM (26% decrease) and 70 μM (18% decrease), respectively. Calcium concentrations decrease smoothly from 10 to 2 mM over the 3 m length of the core. Calcium isotope ratios are close to zero in the upper part of the core, but increase slightly to 0.2‰ between approximately 1.5 and 2.5 mbsf. Carbon isotope ratios in DIC decrease steadily from −4‰ in the shallowest sample (0.05 mbsf) to a minimum of −32‰ at 2.1 mbsf, before rising at greater depths to reach −19‰ at 2.9 mbsf.

Pore fluids from core 1520GC show much more abrupt changes compared to 940GC, with transitions occurring at shallower depths and with steeper gradients. The drop in sulfate and increase in total alkalinity occur sharply between 0.7 and 0.9 mbsf. In contrast to 940GC, magnesium remains essentially constant with depth, but strontium concentrations also decrease to 63 μM (28% decrease). Calcium concentrations drop to 3 mM over the same interval that sulfate decreases, while calcium isotope ratios increase to 0.4‰. Carbon isotope ratios of DIC decrease with depth to −32‰, the same minimum value observed at 940GC, but at the much shallower depth of 0.9 mbsf. At greater depths in 1520GC, $\delta^{13}C$ values of DIC rise towards positive values, reaching 8‰ at 3.4 mbsf.

Based on comparisons between the shallowest pore fluid samples (5 and 3 cm below the sediment-water interface for 940GC and 1520GC, respectively) and the composition of seawater, there is no resolvable offset in major ion concentrations (Hong et al., 2017, 2018) or in calcium isotope ratios for pore fluids, indicating that pore fluid collection by Rhizons did not induce any sampling-related artifacts. The strong apparent gradient in carbon isotope ratios across the sediment-water interface prevents such a comparison and assessment of sampling artifacts for measured $\delta^{13}C$ values in the pore fluids, so a 0–1‰ offset towards more positive values (Steiner et al., 2018) may be present in the pore fluid $\delta^{13}C$ data presented here. However, the magnitude of this potential offset is small relative to the observed range in $\delta^{13}C$ values in the pore fluid profiles and would have a negligible effect on interpretations of these data.

3.2 Carbonate nodules

Mineralogical and geochemical data from the authigenic carbonate nodules from 1520GC show a composition dominated by Mg-calcite with Mg/Ca ratios ranging from 0.13 to 0.24 mol/mol (Table 3). The geochemical compositions are relatively constant among subsamples of an individual nodule. There is more variation across the set of nodules than within subsamples from the same nodule. Calcium isotope ratios range from −0.86 to −0.30‰ and are positively correlated with Mg/Ca ratios (r^2 = 0.77) with a weak inverse correlation with Sr/Ca ratios (r^2 = 0.44) (Fig. 4).

Compared to methane-derived carbonates recovered at seep sites in the Barents and North Seas (Thiagarajan et al., 2020), the samples from 1520GC show less geochemical variability in all measured properties (Fig. 4).

Quantitative mineralogical assessments from XRD match the predictions from the geochemical patterns (Table 3). Mg-calcite is the dominant carbonate phase, with only one subsample containing a substantial amount (> 1% of total carbonate) of aragonite. This subsample, which consists of 12% aragonite and 55% Mg-calcite, also has the most negative $\delta^{44/40}$Ca values measured in the nodules from 1520GC, −0.86‰, as well as the highest Sr/Ca and lowest Mg/Ca ratios. Minor dolomite (up to 3.7%) that could be either detrital or authigenic is also present in the nodules. Assuming that the calcium carbonate phases are mainly authigenic, 25–42% of each sample consists of detrital sediments, predominantly quartz, mica (clays), and plagioclase, with minor K-feldspar, chlorite, hornblende, and pyrite (in general order of abundance). These acetic-acid-insoluble phases were not dissolved by the treatments described above and do not contribute to the trace element and isotopic results. The composition of the detrital components is roughly constant across all the subsamples.

Previously reported δ^{13}C values of the nodules from 1520GC range from −31 to −23‰ (Hong et al., 2017). These are similar to δ^{13}C values of authigenic carbonates at other active and fossil methane seeps in the Barents and Norwegian Seas (Crémière et al., 2016; Thiagarajan et al., 2020).

4 Discussion

4.1 Evolution of subsurface conditions

The pore fluid profiles from these methane seep sites present special conditions that allow for calculating the effective calcium isotope fractionation and estimating precipitation rate at a specific moment in time. The concave-up and kink-shaped profiles in sulfate concentrations (Fig. 3) show that the flux of subsurface methane has increased recently (on the order of thousands and hundreds of years ago for 940GC and 1520GC, respectively) and that pore fluid profiles are still evolving to-

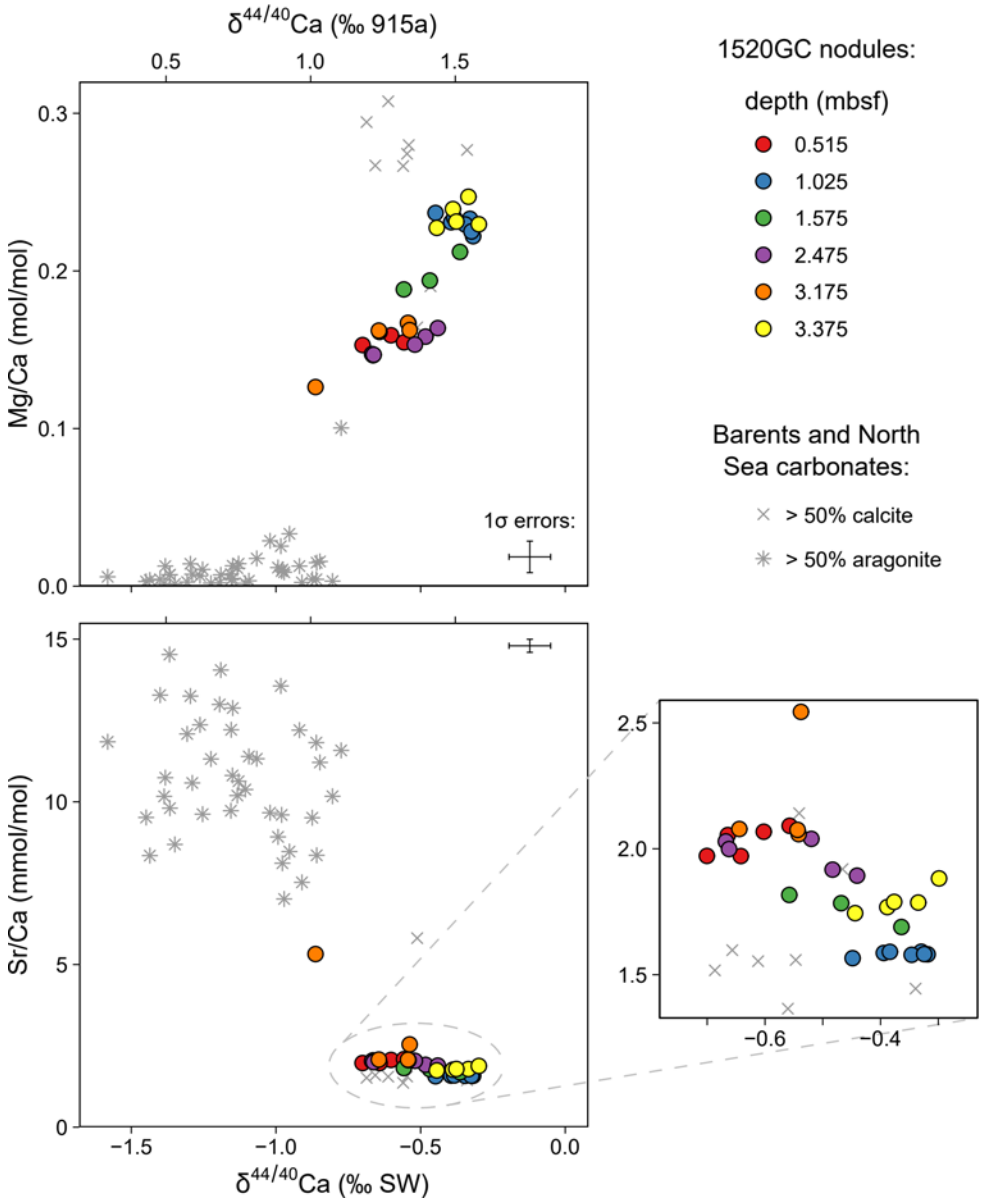

Figure 4: Geochemical properties of authigenic carbonate nodules from 1520GC (colored circles), compared to carbonate crusts from other methane seep sites in the Barents and North Seas (gray symbols) reported in Thiagarajan et al. (2020).

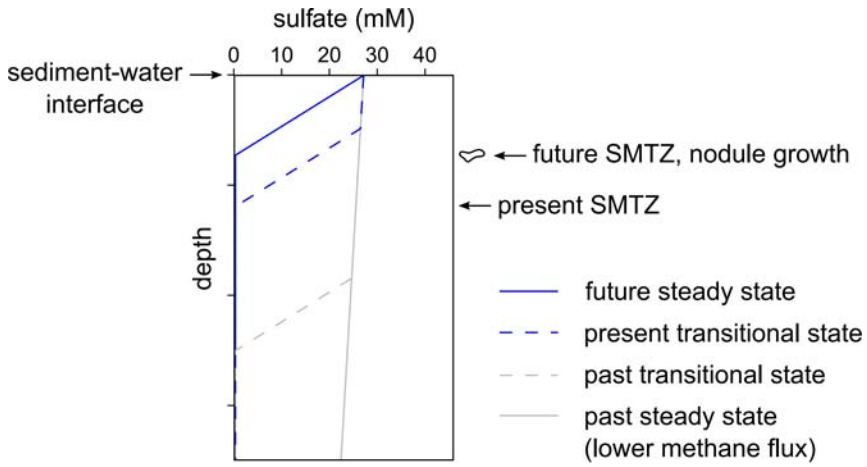

Figure 5: Idealized cartoon representation of pore-fluid evolution of sulfate concentrations and SMTZ migration at study sites. Authigenic carbonate nodules may form when the SMTZ occupies a depth interval for an extended period of time during steady-state conditions, with ions supplied by diffusion from above. During transitional states (including the state captured by the modern pore fluid profiles), carbonate mineral precipitation is volumetrically insignificant and effectively occurs in a closed system, where only ions that are already present in the pore fluids are consumed as the profile evolves upward towards a new steady state defined by a higher methane flux.

wards new steady states (Hong et al., 2017). At steady-state conditions, sulfate concentrations will be controlled by diffusion and decrease linearly with depth towards the sulfate-methane transition zone (SMTZ). In contrast, the non-linear profiles at these two sites indicate upward (and ongoing) migration of the SMTZ (Fig. 5). The rate of sulfate reduction and the location of the SMTZ at steady-state will be determined by the flux of methane from below. The excellent correlation between sulfate and calcium concentrations shows that sulfate reduction coupled to anaerobic oxidation of methane (AOM) leads to calcium drawdown through alkalinity production and precipitation of authigenic carbonate within the SMTZ.

Whereas pore fluid profiles capture a snapshot of presently evolving subsurface conditions, the authigenic carbonate nodules are the reaction products of conditions at these sites over longer intervals of time. The calcium concentration profiles indicate that carbonate minerals precipitate largely within and immediately surrounding the SMTZ, and therefore the depth range over which carbonate nodules are found reflects the past migration of the SMTZ through the sediment column. The SMTZ may move vertically either by accumulation (or erosion) of sediment or changes in the methane flux from below. For example, carbonate nodules found at shallower depths than

the present SMTZ at 1520GC could reflect erosion of sediment or a greater methane flux in the past (Hong et al., 2017). Mass balance considerations also require that the nodules grew over an extended period of time because the drawdown of calcium within the pore fluid profile can only account for a fraction of the carbonate present (in a closed system, the observed decrease of 7 mM calcium would yield less than a milligram of carbonate per cm^3). To grow nodules, calcium must ultimately be supplied by diffusion from the overlying seawater while the SMTZ occupies a particular interval at a stable methane flux level. For present-day fluxes (see section 4.3), growth of cm-scale nodules would require precipitation at the SMTZ over at least 10^2-year timescales.

The carbon isotope ratios of the carbonate nodules compared to DIC also demonstrate how the SMTZ must have migrated in the past. Minimum $\delta^{13}C$ values of $-32‰$ occur for DIC at the SMTZs of both 940GC and 1520GC, reflecting the active oxidation of ^{13}C-depleted methane at those depths. Carbonate nodules from 1520GC have $\delta^{13}C$ values ranging from -31 to $-23‰$; given a $1‰$ carbon isotope fractionation between DIC and calcite (Romanek et al., 1992), these nodules suggest pore fluid $\delta^{13}C$ values were between -32 and $-24‰$ during nodule growth. Measured $\delta^{13}C$ values in the DIC are much higher both shallower and deeper than the modern SMTZ (Fig. 6), indicating that the nodules did not grow under their present conditions, but rather in the past when the SMTZ occupied those sedimentary intervals (Hong et al., 2017). The range of nodule $\delta^{13}C$ values may reflect some limited assimilation of carbon outside of the SMTZ or a different balance of carbon sources (i.e. different proportions of methane-, organic matter-, and seawater-derived DIC within the SMTZ) in the past. The low $\delta^{13}C$ values of the nodules also confirm that detrital sedimentary carbonate (e.g. foraminifera or dolomite grains, with expected $\delta^{13}C$ values close to $\sim 0‰$) is negligible.

4.2 Interpreting pore fluid calcium isotope ratios

The drawdown of calcium as authigenic carbonate precipitates in 940GC and 1520GC fractionates calcium isotope ratios and shapes the pore fluid profiles of $\delta^{44/40}Ca$ values. In a closed system, the preferential removal of lighter calcium isotopes during rapid carbonate precipitation will en-

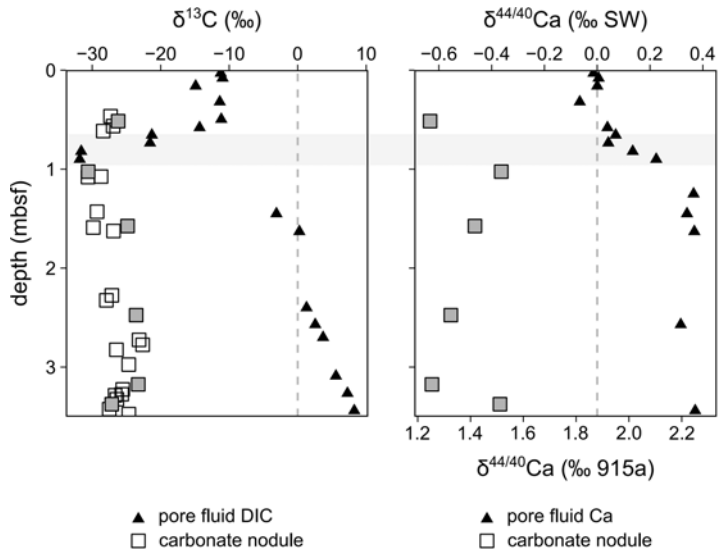

Figure 6: Comparison of carbon isotope ratios ($\delta^{13}C$ values) and calcium isotope ratios ($\delta^{44/40}Ca$ values) for pore fluids and authigenic carbonate nodules (average of multiple subsamples) at 1520GC. Filled squares indicate nodules with $\delta^{44/40}Ca$ values analyzed in this study (nodule $\delta^{13}C$ data previously reported in Hong et al., 2017).

rich pore fluids in the heavier isotopes through Rayleigh distillation, leading pore fluids to evolve towards higher $\delta^{44/40}Ca$ values than in the overlying seawater. The fractionation of calcium isotopes is thought to be the expression of a kinetic isotope effect, based on both experimental and theoretical constraints (Fantle and DePaolo, 2007; Tang et al., 2008; DePaolo, 2011; Nielsen et al., 2012). Aqueous diffusion of calcium within the pore fluid profile generates negligible isotope fractionation (Bourg et al., 2010). In the non-steady-state conditions captured at 940GC and 1520GC, precipitation at the SMTZ is essentially occurring within a closed system, consuming only the available reactant within the pore fluids as the SMTZ migrates towards the surface (see Fig. 5). Diffusion of calcium from the overlying seawater has no influence below the kinks in the pore fluid profiles, below which calcium is being consumed into carbonate minerals. Below the SMTZ, calcium concentrations and isotope ratios are relatively constant (Fig. 3), suggesting that no further net reaction is occurring.

The extent of back reaction between the authigenic carbonate minerals and the pore fluids is unknown, such that only the apparent fractionation associated with the net forward (attachment) and backward (detachment) reactions can be constrained. The over-saturated conditions (see sec-

tion 4.3) and the rapid decrease in calcium concentrations at the SMTZ show that the forward reaction is more important, but the balance between the net and gross precipitation rates cannot be further quantified in this setting. If isotopic exchange or re-equilibration with the authigenic carbonate minerals is important, calcium isotope ratios in the pore fluids would be lower than for a unidirectional reaction (e.g. Fantle and DePaolo (2007); Jacobson and Holmden (2008); Teichert et al. (2009)), and the apparent fractionations derived below would be smaller than (i.e. closer to equilibrium than) the fractionation associated with the forward precipitation reaction only. However, in carbonate-rich marine sediments, calcium isotopic equilibrium with sedimentary carbonate minerals is only achieved on a million-year timescale (Fantle and DePaolo, 2007), suggesting that the young Holocene cores sampled here with minor carbonate mineral components would not have experienced significant re-equilibration. Within these constraints, the pore fluids at 940GC and 1520GC can be used to estimate the apparent fractionation factor using a Rayleigh distillation model:

$$\frac{R_f}{R_0} = f^{(\alpha-1)}$$

where R_f is the calcium isotope ratio ($^{44}Ca/^{40}Ca$) of the distilled pore fluid, R_0 is the calcium isotope ratio of the initial pore fluid (assumed to be equal to the ratio in seawater, which is consistent with the measured values in the shallowest parts of the profiles, see Fig. 3), f is the fraction of calcium removed (relative to the concentration in seawater), and α is the net calcium isotope fractionation factor ($\alpha = R_{\text{carbonate}}/R_{\text{fluid}}$).

Previous studies have suggested that Rayleigh distillation could explain the variation observed in carbonate mineral deposits associated with methane hydrates and methane seeps (Teichert et al., 2005; Wang et al., 2012), but these inferences were made in the absence of measured pore fluid compositions and required assuming a constant calcium isotope fractionation factor determined under very different environmental conditions. For example, a range of $\delta^{44/40}Ca$ values (−1.4 to −0.7‰, converted to the seawater scale) was observed in aragonite precipitates in direct association with gas hydrates (Teichert et al., 2005). However, the observed range could equally be

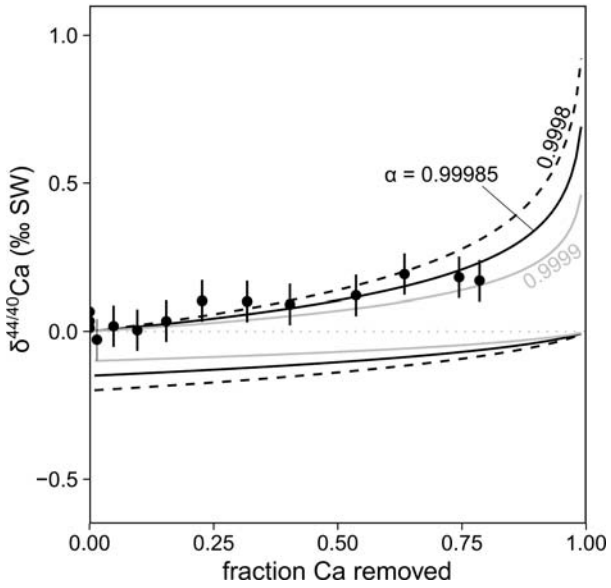

Figure 7: Rayleigh distillation model applied to pore fluid data from 940GC. Upper curves show pore fluid composition (best fit $\alpha = 0.99985$); lower curves show the integrated product (authigenic carbonate minerals). Error bars represent 1σ analytical error.

explained by variability in the fractionation factor. In a separate organic-rich sedimentary environment bearing authigenic high-Mg calcite nodules with an apparent fractionation factor of α = 0.9994–0.9992, Rayleigh distillation was expected but not observed in the pore fluids, possibly because of overprinting effects from other sedimentary processes (Teichert et al., 2009). Compared to these previous approaches, the high-resolution sampling of pore fluids at sites 940GC and 1520GC under the special conditions of rapid, non-steady-state authigenic carbonate precipitation provides an opportunity to observe this mechanism at work and resolve the magnitude of calcium isotope fractionation at these locations.

At 940GC, pore fluids are only slightly enriched in the heavier isotopes of calcium despite the substantial decrease in calcium concentration. This relationship defines a best-fit apparent fractionation factor of $\alpha = 0.99985$ (Fig. 7). For a similar change in calcium concentration, the pore fluids at 1520GC have much higher $\delta^{44/40}$Ca values, with a best fit of $\alpha = 0.9996$ (Fig. 8). The different magnitudes of the apparent fractionation factors between fluid and precipitate expressed at these sites may be caused by different precipitation rates related to the methane fluxes and also expressed in the abruptness of the concentration gradients in the pore fluid profiles (see section

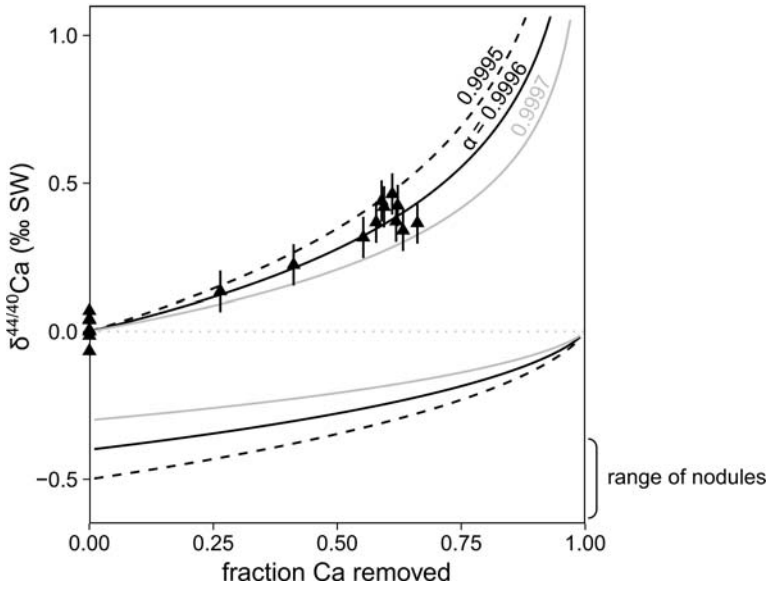

Figure 8: Rayleigh distillation model applied to pore fluid data from 1520GC. Upper curves show pore fluid composition (best fit $\alpha = 0.9996$); lower curves show the integrated product (authigenic carbonate minerals). Error bars represent 1σ analytical error.

4.3 below). Given the location of active methane seepage atop the seafloor mound (Fig. 1), this relationship is consistent with the greater distance between core 940GC and the top of the mound compared to 1520GC yielding a lower methane flux, lower precipitation rates, and smaller calcium isotope fractionation.

4.3 Relating calcium isotope fractionation to precipitation rate

Although the pore fluid profiles at these sites are presently out of steady state, the gradients preserved within specific intervals can be interpreted to estimate precipitation rates at the current locations of the SMTZ. The calcium concentration gradients below the kinks in the profiles are used to quantify the flux of calcium per unit surface area into the SMTZ following Fick's first law of diffusion for a 1D system:

$$F = -D\frac{dC}{dz} \tag{1}$$

where F is the downward calcium flux, D is the apparent diffusivity ($D = D_0/\theta^2$, where D_0 is

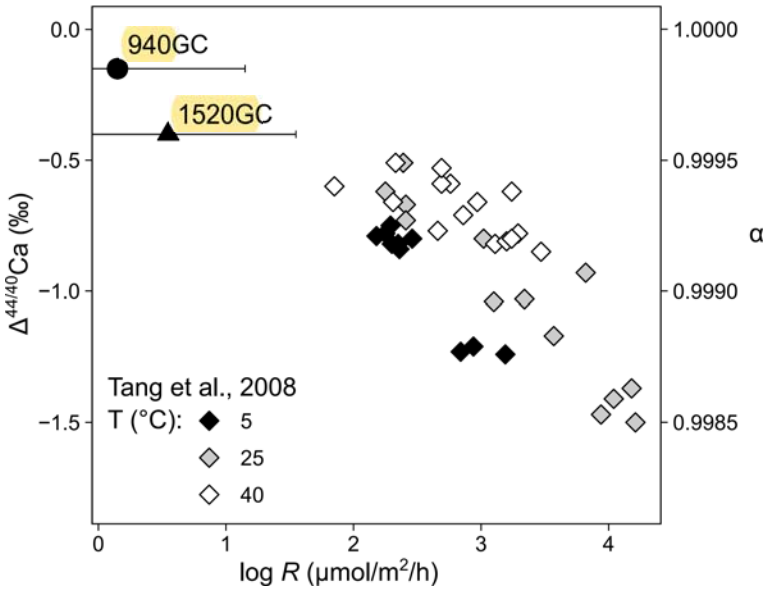

Figure 9: Comparison of calcite precipitation rates (R, per unit reactive surface area) and isotopic fractionation between calcite and aqueous fluid ($\Delta^{44/40}$Ca, α) from sites in this study and laboratory experimental data (Tang et al., 2008). For sites in this study, isotopic fractionations are calculated from a Rayleigh distillation model (section 4.2, Fig. 7,8); precipitation rates are estimated from calcium fluxes scaled to estimates of reactive surface area at the SMTZ interface at a temperature of 0 °C, with uncertainty of approximately an order of magnitude in either direction.

the estimated infinite-dilution diffusion coefficient and θ is tortuosity), and C is the concentration with z positive downwards (Boudreau, 1997). Tortuosity is estimated from porosity (ϕ) by the relation $\theta^2 = 1 - \ln(\phi^2)$. Assuming a temperature of 0 °C and $\phi = 0.7$ for conditions in the Storfjordrenna region (Hong et al., 2017), D is estimated to be 7.6×10^{-7} m^2/h. For 940GC, where a decrease in calcium concentrations of 7 mM occurs over approximately 1.5 m above the SMTZ, the flux of calcium into the SMTZ is estimated to be 3.5 μmol/m^2/h. For 1520GC, where a similar decrease occurs over 0.6 m, the flux is estimated to be 8.8 μmol/m^2/h per unit seafloor area.

Relating these calcium fluxes to estimated precipitation rates of calcium carbonate per unit reactive surface area in the natural environment requires several assumptions and rough estimates. Calcium carbonate precipitation is assumed to occur at a theoretical planar interface at the SMTZ, driven by AOM. A common approach for estimating reactive surface area for a given volume of sediment, when not measured by gas adsorption methods, for example, uses the geometrical sur-

face area (a function of grain size and shape) scaled by a roughness factor and a surface reactivity factor (Beckingham et al., 2016). Adapting this approach to the methane seep sites, where the volume of sediment involved in the reaction is undefined, the reactive surface area is taken to be the geometrical estimate of a subsurface horizontal plane (equal to the seafloor surface area used in the flux calculation above) multiplied by these two scaling factors. General values used for the roughness factor for fine-grained sediments are 10 and 160 (Zerai et al., 2006; Maher et al., 2009), while the surface reactivity factor has broad uncertainty and is estimated to be between 0.1 and 0.001 (Beckingham et al., 2016). Taking the geometric means of these ranges, the combined scaling factors yield a factor of 0.4 to convert calcium fluxes at the seafloor to calcium carbonate precipitation rates on available mineral surface area at the SMTZ. This calculation yields precipitation rates, R, per unit reactive surface area of 1.4 μmol/m^2/h at 940GC and 3.5 μmol/m^2/h at 1520GC. Uncertainties on estimating reactive surface area should be considered to be an order of magnitude in either direction, noting also that this method does not capture the lateral variability, possibly driven by nucleation kinetics, that must exist for growth of nodules rather than continuous horizons of authigenic carbonate.

These estimated precipitation rates of calcium carbonate within the present-day SMTZ are one to three orders of magnitude lower than precipitation rates achieved in the laboratory experiments of Tang et al. (2008) (Fig. 9). With the fractionation factors assessed from the pore fluid profiles of calcium isotope ratios (Figs. 7 and 8), sites 1520GC and 940GC continue the trend observed for experimentally grown calcite with greater isotopic fractionation at higher precipitation rates and smaller fractionation at slower rates. Calcium carbonate saturation is not directly comparable between the experimental and environmental settings: the saturation index ($SI_{calcite} = \log(IAP/K_{sp,calcite})$, where IAP is the ion activity product and K_{sp} is the thermodynamic solubility product) was between 0.51 and 1.23 in the experiments of Tang et al. (2008) whereas it is estimated to be 1.35 within the SMTZ at the methane seep sites, based on results from a comprehensive pore-fluid chemistry model for a core site atop the mound a few hundred meters from 940GC and 1520GC (Fig. 1) and with similar pore fluid profiles (911GC in Hong et al., 2017).

However, these methane seep sites are one of the first natural environments where the active relationship between inorganic calcite precipitation rate and calcium isotope fractionation can be quantified at conditions far enough from equilibrium to impart measurable isotopic fractionation. These results may in turn be used to help refine the parameters of theoretical models of isotopic fractionation during calcite precipitation (e.g. DePaolo, 2011; Nielsen et al., 2012). For example, the equilibrium fractionation for infinitely low precipitation rates must be closer to 1 than $\alpha = 0.99985$, based on the observations from 940GC. Notably, there appears to be less isotope fractionation at the methane seep sites than at near-equilibrium conditions where recrystallizing carbonate sediments within a deep drillcore were inferred to express $\alpha = 0.9995$ (Bradbury and Turchyn, 2018). This suggests that different settings may express different relationships between precipitation rate and calcium isotope fractionation, potentially reflecting the importance of other fluid properties, environmental conditions, or mineral surface parameters. Differences in the direction of the relationship shown in Fig. 9 have also been observed under different experimental conditions (Lemarchand et al., 2004; AlKhatib and Eisenhauer, 2017), showing less isotopic fractionation at higher precipitation rates. It has been suggested that an extremely ammonium-rich solution matrix could have changed the complexing behavior and desolvation kinetics, and therefore isotopic fractionation, of calcium ions in those experiments (AlKhatib and Eisenhauer, 2017), but further investigation is needed to fully understand the parameters that are important for shaping the relationship between calcium isotope fractionation and precipitation rate in natural environments.

4.4 Interpreting carbonate nodule geochemistry

Despite the different timescales reflected by the pore fluids (reactions occurring presently within the sediment column, not in steady-state) and the carbonate nodules (conditions integrated over longer periods of time at the past locations of the SMTZ), a comparison of their geochemistry provides additional constraints on the evolution of the methane seep system. The geochemical homogeneity within subsamples of a nodule (Fig. 4) indicates that entire nodules grew under relatively stable ambient pore fluid conditions; differences among the individual nodules show that

those conditions changed over time. This observation supports the idea that variability in nodule $\delta^{13}C$ values is related to different proportions of DIC derived from the two dominant sources, methane oxidation and diffused or buried seawater, as opposed to carbonate precipitation at depths outside of the SMTZ, which would be expected to generate spatial heterogeneity in $\delta^{13}C$ values. These proportions are controlled by the methane flux, which will establish the SMTZ (where nodules will grow) at the depth where sufficient sulfate for AOM is supplied by diffusion. The rate of AOM will in turn influence the rate of authigenic carbonate precipitation.

The nodules measured at 1520GC have $\delta^{44/40}Ca$ values lower than would be expected given the fractionation factors expressed in modern pore fluid profiles (Fig. 8). The fraction of calcium consumed during the steady-state, open-system precipitation of the nodules is unknown, preventing a precise estimate of the isotopic fractionation factor, but the average $\delta^{44/40}Ca$ values for each nodule of -0.36 to $-0.63‰$ define the maximum possible values for α (corresponding to small f) of 0.99964 to 0.99937, with lower values likely. This difference suggests that the nodules grew at faster precipitation rates than those supported by the present diffusive flux of calcium, corresponding to higher methane fluxes and a shallower SMTZ. The nodules recovered at shallower depths than the modern SMTZ are consistent with this interpretation (see Fig. 6), although their presence could also be explained by surface erosion. Although the history of methane seepage in this region cannot be fully reconstructed, it is possible that pulses of higher methane flux capable of supporting the growth of authigenic carbonate nodules were episodic, which would also be consistent with the presence of nodules at discontinuous intervals throughout the core. At Hydrate Ridge (offshore Oregon, USA), variable $\delta^{44/40}Ca$ values reported in carbonate crusts directly associated with methane hydrate deposits (Teichert et al., 2005) may similarly be caused by different fractionation factors related to the rate of methane oxidation. This interpretation differs from the previous hypothesis for those deposits (Teichert et al., 2005) that pore fluids in that setting evolved towards very high $\delta^{44/40}Ca$ values (up to $0.8‰$ heavier than seawater), which would be challenging to maintain with the mass balance requirement of supplying calcium by diffusion for the carbonate crusts. These two possibilities, rate-dependent isotope fractionation or ^{44}Ca-enriched pore fluids,

could potentially be tested with trace element analyses of the crusts.

For the authigenic carbonates at 1520GC, variable precipitation rates, as interpreted from their $\delta^{44/40}$Ca values, also correlate with variations in trace element composition and mineralogy. Faster rates (lower $\delta^{44/40}$Ca values) yield lower Mg/Ca ratios and higher Sr/Ca ratios (Fig. 4), and also correspond to higher proportions of aragonite. Contributions from aluminosilicates or other non-carbonate phases appear to be negligible based on the lack of correlation between measured Mg/Ca and Al, Li, or Mn concentrations, for example (Table 3). The observed relationships within the carbonate nodules likely include the combined effects of three factors, all of which are potentially functions of precipitation rate: 1) changing distribution coefficients for a given carbonate polymorph, 2) precipitation of a mix of Mg-calcite and aragonite, and 3) changing pore fluid Mg/Ca and Sr/Ca within the SMTZ. The importance of changing distribution coefficients for Mg-calcite is suggested by the correlations between Mg/Ca, Sr/Ca, and $\delta^{44/40}$Ca values where Mg-calcite is the dominant authigenic phase (< 1% or no detectable aragonite). In contrast, the composition of the subsample with the highest fraction of aragonite measured is most likely the result of its mineralogy, as is much of the variability observed in seafloor methane-derived carbonate crusts analyzed from the Barents and North Seas (Thiagarajan et al., 2020) (Fig. 4). These observations are consistent with models that suggest connections between calcium isotope fractionation and trace element distributions are linked to the kinetics of ion desolvation and attachment (Gussone et al., 2005; Tang et al., 2008; DePaolo, 2011; Nielsen et al., 2012). However, it is not clear how important these effects are generally for other (e.g. biogenic) carbonates, since the variations in precipitation rates for these inorganic methane-seep carbonates are externally controlled and more extreme compared to many other settings of carbonate precipitation. Changes in pore fluid Mg/Ca and Sr/Ca, which are not known for the time intervals when the nodules grew, may also contribute to some of the variability in the nodules. In the present day SMTZ at 1520GC, the elevated molar Mg/Ca ratio of 13 (2.5 times the ratio in seawater) and Sr/Ca ratio of 0.016 (2 times the ratio in seawater) are primarily driven by the drawdown of calcium, with much smaller relative decreases in magnesium and strontium concentrations (Fig. 3). Variation in these ratios over time during

periods of nodule growth cannot be ruled out, but their similarity at the two sites, 940GC and 1520GC, despite different methane fluxes and precipitation rates, suggests that they may not be the dominant contribution to trace element variability of the authigenic nodules.

Precipitation rate may also partly determine which polymorph of calcium carbonate forms, which can explain some fraction of the geochemical variability in the 1520GC nodules. Both aragonite and Mg-calcite are common authigenic precipitates at methane seeps. A variety of physicochemical parameters influence which mineral phase forms, with methane flux and ambient sulfate concentrations exerting a strong control (Greinert et al., 2001; Peckmann et al., 2001). Aragonite precipitation typically occurs under high methane flux conditions with a shallow SMTZ near the sediment-water interface where sulfate is abundant, which can result in carbonate-cemented seafloor crusts where aragonite forms fibrous cement and/or fills cavities (Crémière et al., 2016). On the other hand, Mg-calcite (up to 20 mol% Mg) forms under lower methane flux when the SMTZ is within subsurface sediments and porewater sulfate is relatively low (Naehr et al., 2007). Spotty cementation of detrital sediments by micritic Mg-calcite results in formation of nodules like those seen at the Storfjordrenna sites. In the Barents and North Seas, carbonate crusts containing both aragonite and Mg-calcite were recovered from methane seeps, with petrographic evidence that the aragonite formed at higher methane fluxes and precipitation rates (Thiagarajan et al., 2020). For those crusts, rapid precipitation rates were also required to explain disequilibrium isotope effects observed in carbonate clumped isotope measurements for certain aragonite phases (Thiagarajan et al., 2020). The nodules from 1520GC overlap with a limited fraction of the compositional variability observed in the Barents and North Sea seep carbonates (Fig. 4), indicating consistent mineralogical and kinetic effects shared across these samples.

5 Conclusions

Previous experimental and theoretical work has shown that calcium isotope fractionation in calcium carbonate minerals is a function of mineralogy and precipitation rate. This study demon-

strates the expression of these relationships in a natural setting where authigenic carbonate is precipitating at a methane seep site in the northern Barents Sea near Svalbard. This setting allows for the quantification of carbonate precipitation rates driven by the anaerobic oxidation of methane within the sediment column through analysis of pore fluid geochemical profiles. The pore fluid profiles show elevated calcium isotope ratios from precipitation of authigenic carbonate with calcium isotope fractionation factors of α = 0.9996 to 0.99985, a smaller magnitude of calcium isotope fractionation than expressed in typical marine carbonates. The range of observed fractionations reflects different rates of precipitation driven by variable methane fluxes and rates of anaerobic oxidation of methane. The variation in precipitation rate also affects the trace element composition of the carbonates (Mg/Ca and Sr/Ca ratios), as well as the polymorph of calcium carbonate (Mg-calcite versus aragonite). This system of inorganic carbonate precipitation provides the necessary constraints for distinguishing multiple controls on geochemical variability and confirming mechanisms of calcium isotope fractionation in these mineral archives.

Acknowledgments

The authors would like to acknowledge the captains and crews onboard R/V Helmer Hanssen for cruises CAGE15-2 and CAGE15-6 and thank the chief scientists Dr. Giuliana Panieri (CAGE15-2) and Dr. Jürgen Mienert (CAGE15-6). This work was supported by the Research Council of Norway through its Centres of Excellence funding scheme (project number 223259) and NORCRUST (project number 255150).

References

AlKhatib, M. and Eisenhauer, A. (2017) Calcium and strontium isotope fractionation in aqueous solutions as a function of temperature and reaction rate; I. Calcite. *Geochimica et Cosmochimica Acta* 209:296–319.

510 Andersen, E. S., Dokken, T. M., Elverhøi, A., Solheim, A., and Fossen, I. (1996) Late Quaternary
511 sedimentation and glacial history of the western Svalbard continental margin. *Marine Geology*
512 133:123–156.

513 Beckingham, L. E., Mitnick, E. H., Steefel, C. I., Zhang, S., Voltolini, M., Swift, A. M., Yang,
514 L., Cole, D. R., Sheets, J. M., Ajo-Franklin, J. B., DePaolo, D. J., Mito, S., and Xue, Z. (2016)
515 Evaluation of mineral reactive surface area estimates for prediction of reactivity of a multi-
516 mineral sediment. *Geochimica et Cosmochimica Acta* 188:310–329.

517 Bischoff, W. D., Bishop, F. C., and Mackenzie, F. T. (1983) Biogenically produced magnesian
518 calcite: Inhomogeneities in chemical and physical properties; comparison with synthetic phases.
519 *American Mineralogist* 68:1183–1188.

520 Blättler, C. L., Henderson, G. M., and Jenkyns, H. C. (2012) Explaining the Phanerozoic Ca
521 isotope history of seawater. *Geology* 40:843–846.

522 Blättler, C. L. and Higgins, J. A. (2017) Testing Urey's carbonate–silicate cycle using the calcium
523 isotopic composition of sedimentary carbonates. *Earth and Planetary Science Letters* 479:241–
524 251.

525 Blättler, C. L., Higgins, J. A., and Swart, P. K. (2019) Advected glacial seawater preserved in the
526 subsurface of the Maldives carbonate edifice. *Geochimica et Cosmochimica Acta* 257:80–95.

527 Boudreau, B. P. (1997) *Diagenetic models and their implementation; modelling transport and*
528 *reactions in aquatic sediments*. Springer, Berlin.

529 Bourg, I. C., Richter, F. M., Christensen, J. N., and Sposito, G. (2010) Isotopic mass dependence of
530 metal cation diffusion coefficients in liquid water. *Geochimica et Cosmochimica Acta* 74:2249–
531 2256.

532 Bradbury, H. J. and Turchyn, A. V. (2018) Calcium isotope fractionation in sedimentary pore fluids

from ODP Leg 175: Resolving carbonate recrystallization. *Geochimica et Cosmochimica Acta* 236:121–139.

Crémière, A., Lepland, A., Chand, S., Sahy, D., Condon, D. J., Noble, S. R., Martma, T., Thorsnes, T., Sauer, S., and Brunstad, H. (2016) Timescales of methane seepage on the Norwegian margin following collapse of the Scandinavian Ice Sheet. *Nature Communications* 7:11509.

DePaolo, D. J. (2011) Surface kinetic model for isotopic and trace element fractionation during precipitation of calcite from aqueous solutions. *Geochimica et Cosmochimica Acta* 75:1039–1056.

Fantle, M. S. and DePaolo, D. J. (2007) Ca isotopes in carbonate sediment and pore fluid from ODP Site 807A: The Ca^{2+}(aq)–calcite equilibrium fractionation factor and calcite recrystallization rates in Pleistocene sediments. *Geochimica et Cosmochimica Acta* 71:2524–2546.

Fantle, M. S. and Tipper, E. T. (2014) Calcium isotopes in the global biogeochemical Ca cycle: Implications for development of a Ca isotope proxy. *Earth-Science Reviews* 129:148–177. doi:10.1016/j.earscirev.2013.10.004.

Greinert, J., Bohrmann, G., and Suess, E. (2001) Gas hydrate-associated carbonates and methane-venting at Hydrate Ridge: classification, distribution and origin of authigenic lithologies. *Geophysical Monograph-American Geophysical Union* 124:99–114.

Gussone, N., Böhm, F., Eisenhauer, A., Dietzel, M., Heuser, A., Teichert, B. M. A., Reitner, J., Wörheide, G., and Dullo, W.-C. (2005) Calcium isotope fractionation in calcite and aragonite. *Geochimica et Cosmochimica Acta* 69:4485–4494.

Gussone, N., Eisenhauer, A., Heuser, A., Dietzel, M., Bock, B., Böhm, F., Spero, H. J., Lea, D. W., Bijma, J., and Nägler, T. F. (2003) Model for kinetic effects on calcium isotope fractionation (δ^{44}Ca) in inorganic aragonite and cultured planktonic foraminifera. *Geochimica et Cosmochimica Acta* 67:1375–1382.

Gussone, N., Hönisch, B., Heuser, A., Eisenhauer, A., Spindler, M., and Hemleben, C. (2009) A critical evaluation of calcium isotope ratios in tests of planktonic foraminifers. *Geochimica et Cosmochimica Acta* 73:7241–7255.

Heuser, A. and Eisenhauer, A. (2008) The calcium isotope composition ($\delta^{44/40}$Ca) of NIST SRM 915b and NIST SRM 1486. *Geostandards and Geoanalytical Research* 32:311–315.

Heuser, A., Schmitt, A.-D., Gussone, N., and Wombacher, F. (2016) *Analytical Methods*, pages 23–73. Springer Berlin Heidelberg, Berlin, Heidelberg.

Hippler, D., Schmitt, A.-D., Gussone, N., Heuser, A., Stille, P., Eisenhauer, A., and Nägler, T. F. (2003) Calcium isotopic composition of various reference materials and seawater. *Geostandards Newsletter* 27:13–19.

Hong, W.-L., Torres, M. E., Carroll, J., Crémière, A., Panieri, G., Yao, H., and Serov, P. (2017) Seepage from an arctic shallow marine gas hydrate reservoir is insensitive to momentary ocean warming. *Nature Communications* 8:15745.

Hong, W.-L., Torres, M. E., Portnov, A., Waage, M., Haley, B., and Lepland, A. (2018) Variations in gas and water pulses at an Arctic seep: fluid sources and methane transport. *Geophysical Research Letters* 45:4153–4162.

Jacobson, A. D., Andrews, M. G., Lehn, G. O., and Holmden, C. (2015) Silicate versus carbonate weathering in Iceland: New insights from Ca isotopes. *Earth and Planetary Science Letters* 416:132–142.

Jacobson, A. D. and Holmden, C. (2008) δ^{44}Ca evolution in a carbonate aquifer and its bearing on the equilibrium isotope fractionation factor for calcite. *Earth and Planetary Science Letters* 270:349–353.

Lemarchand, D., Wasserburg, G. J., and Papanastassiou, D. A. (2004) Rate-controlled calcium

isotope fractionation in synthetic calcite. *Geochimica et Cosmochimica Acta* 68:4665–4678. doi:10.1016/ j.gca.2004.05.029.

Maher, K., Steefel, C. I., White, A. F., and Stonestrom, D. A. (2009) The role of reaction affinity and secondary minerals in regulating chemical weathering rates at the Santa Cruz Soil Chronosequence, California. *Geochimica et Cosmochimica Acta* 73:2804–2831.

Naehr, T. H., Eichhubl, P., Orphan, V. J., Hovland, M., Paull, C. K., Ussler III, W., Lorenson, T. D., and Greene, H. G. (2007) Authigenic carbonate formation at hydrocarbon seeps in continental margin sediments: A comparative study. *Deep Sea Research Part II: Topical Studies in Oceanography* 54:1268–1291.

Nielsen, L. C., DePaolo, D. J., and De Yoreo, J. J. (2012) Self-consistent ion-by-ion growth model for kinetic isotopic fractionation during calcite precipitation. *Geochimica et Cosmochimica Acta* 86:166–181.

Peckmann, J., Reimer, A., Luth, U., Luth, C., Hansen, B. T., Heinicke, C., Hoefs, J., and Reitner, J. (2001) Methane-derived carbonates and authigenic pyrite from the northwestern Black Sea. *Marine geology* 177:129–150.

Romanek, C. S., Grossman, E. L., and Morse, J. W. (1992) Carbon isotopic fractionation in synthetic aragonite and calcite: effects of temperature and precipitation rate. *Geochimica et Cosmochimica Acta* 56:419–430.

Skulan, J., DePaolo, D. J., and Owens, T. L. (1997) Biological control of calcium isotopic abundances in the global calcium cycle. *Geochimica et Cosmochimica Acta* 61(12):2505–2510.

Steiner, Z., Lazar, B., Erez, J., and Turchyn, A. V. (2018) Comparing Rhizon samplers and centrifugation for pore-water separation in studies of the marine carbonate system in sediments. *Limnology and Oceanography: Methods* 16:828–839.

603 Tada, R., Murray, R. W., Alvarez Zarikian, C. A., and the Expedition 346 Scientists (2015) Site
604 U1425. In *Proceedings of the Integrated Ocean Drilling Program*, volume 346. International
605 Ocean Discovery Program, College Station, TX.

606 Tang, J., Dietzel, M., Böhm, F., Köhler, S. J., and Eisenhauer, A. (2008) Sr^{2+}/Ca^{2+} and $^{44}Ca/^{40}Ca$
607 fractionation during inorganic calcite formation: II. Ca isotopes. *Geochimica et Cosmochimica*
608 *Acta* 72:3733–3745.

609 Tang, J., Niedermayr, A., Köhler, S. J., Böhm, F., Kısakürek, B., Eisenhauer, A., and Dietzel, M.
610 (2012) Sr^{2+}/Ca^{2+} and $^{44}Ca/^{40}Ca$ fractionation during inorganic calcite formation: III. Impact of
611 salinity/ionic strength. *Geochimica et Cosmochimica Acta* 77:432–443.

612 Teichert, B. M., Gussone, N., Eisenhauer, A., and Bohrmann, G. (2005) Clathrites: archives of
613 near-seafloor pore-fluid evolution ($\delta^{44/40}$Ca, δ^{13}C, δ^{18}O) in gas hydrate environments. *Geology*
614 33:213–216.

615 Teichert, B. M., Gussone, N., and Torres, M. E. (2009) Controls on calcium isotope fractionation
616 in sedimentary porewaters. *Earth and Planetary Science Letters* 279:373–382.

617 Thiagarajan, N., Crémière, A., Blättler, C., Lepland, A., Kirsimäe, K., Higgins, J. A., Brunstad,
618 H., and Eiler, J. (2020) Stable and clumped isotope characterization of authigenic carbonates in
619 methane cold seep environments. *Geochimica et Cosmochimica Acta* 279:204–219.

620 Torres, M. E., Mix, A. C., and Rugh, W. D. (2005) Precise δ^{13}C analysis of dissolved inorganic
621 carbon in natural waters using automated headspace sampling and continuous-flow mass spec-
622 trometry. *Limnology and Oceanography: Methods* 3:349–360.

623 Wang, S., Yan, W., Magalhães, H. V., Chen, Z., Pinheiro, M. L., and Gussone, N. (2012) Calcium
624 isotope fractionation and its controlling factors over authigenic carbonates in the cold seeps of
625 the northern South China Sea. *Chinese Science Bulletin* 57:1325–1332.

626 Wittke, A., Gussone, N., M¨ärz, C., and Teichert, B. M. A. (2020) The effect of extraction tech-
627 niques on calcium concentrations and isotope ratios of marine pore water. *Isotopes in Environ-*
628 *mental and Health Studies* 56:51–68.

629 Young, E. D., Galy, A., and Nagahara, H. (2002) Kinetic and equilibrium mass-dependent isotope
630 fractionation laws in nature and their geochemical and cosmochemical significance. *Geochimica*
631 *et Cosmochimica Acta* 66:1095–1104.

632 Zerai, B., Saylor, B. Z., and Matisoff, G. (2006) Computer simulation of CO_2 trapped through
633 mineral precipitation in the Rose Run Sandstone, Ohio. *Applied Geochemistry* 21(2):223 – 240.

634 Zhang, F., Xu, H., Konishi, H., and Roden, E. E. (2010) A relationship between d_{104} value and
635 composition in the calcite-disordered dolomite solid-solution series. *American Mineralogist*
636 95:1650–1656.